Preprints (www.preprints.org) | NOT PEER-REVIEWED | Posted: 8 April 2022 doi:10.20944/preprints202204.0067.v1

Article

Multi-Scale Modelling of Fuel Droplet Heating and Evaporation in Combustion Engines

Jianfei Xie [1,*]

[1] School of Computing and Engineering, University of Derby, Derby DE22 3AW, United Kingdom; j.xie@derby.ac.uk
* Correspondence: j.xie@derby.ac.uk

Abstract: This review summarises the main numerical models of fuel droplet heating and evaporation (DHE) in combustion engines across the different scales by accessing the nano/micro, meso and macroscopic fluid elements. The phenomena of multi-physics, multi-scale and multi-phase fluid flow and heat transfer are fully investigated when the fuel droplet (dodecane) is heating and evaporated into a background gas (nitrogen) crossing the liquid-vapour (LV) interface, kinetic region (i.e., Knudsen layer) and the bulk regions of liquid and gas in terms of molecular dynamics (MD) simulations, kinetic theory modelling (i.e., direct numerical solutions of Boltzmann equations) and convectional fluid dynamics approach, respectively. The evaporation coefficient of fuel evaporating molecules and their velocity distributions at the LV interface derived from MD simulations formulate a new kinetic boundary condition (KBC). Moreover, a novel kinetic model considering the inelastic collision between fuel molecules alongside the new KBC enables us to describe the non-equilibrium gas dynamics of fuel vapour and gas mixture in Knudsen layer (KL). Heat and mass flux analysis of the fuel droplet under combustion engine conditions can be accurately assessed by implementing the inelastic collision between fuel molecules in KL and a temperature-dependent evaporation coefficient at the LV interface into DHE. The surface temperature of fuel droplet and its evaporation time, which play a significant role in resolving the ignition delay and hence the combustion phasing in engines, can also be well estimated. The multi-scale modelling of fuel DHE will make significantly potential input into the cleaner engine targeting the low-carbon emissions and enhance the capability of the existing computational fluid dynamics (CFD) solvers.

Keywords: fuel droplet; liquid-vapour interface; molecular dynamics; evaporation coefficient; Knudsen layer; kinetic theory modelling

1. Introduction

Lockdown measures prompted a clear fall in the planet air pollution as a result of the less time spent in vehicles during the pandemic. In the first two decades of the 21^{st} century, a large portion of the world's power still comes from burning fossil fuels and burning oil-based fuels generates most of the greenhouse gas emissions as well as being a major pollutant concerned by the United Nations. Nearly all forms of transport vehicles rely on liquid fossil fuels and the use of fossil fuels is likely to continue in the next decade. Therefore, reduction of the fuel consumption in internal combustion (IC) engines and CO_2 emissions produced by transport vehicles (i.e., powertrains and lorries) and off-road carriers (i.e., ships) are of great importance. Hydrocarbon fuels, particularly the diesel fuel, is responsible for the CO_2 emissions and is blamed for producing soot. This needs us to better understand the fuel spray and droplets processes, which can offer smart fuel economy and low carbon missions for the environment in combustion industries. As a primary stage, exploring the heating and evaporation of fuel droplets in compression-ignition engines can help resolve the CO_2 emissions and soot in combustion

© 2022 by the author(s). Distributed under a Creative Commons CC BY license.

Preprints (www.preprints.org) | NOT PEER-REVIEWED | Posted: 8 April 2022 doi:10.20944/preprints202204.0067.v1

phasing. The main purpose of this review is to advance a state-of-the-art investigation of the fuel droplet heating and evaporation (DHE) process in realistic engine conditions.

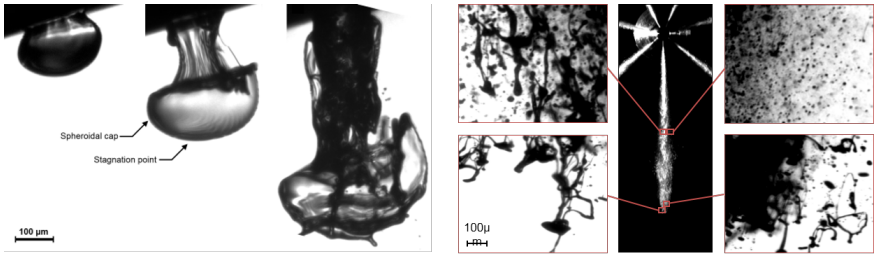

Figure 1. Fuel spray (left panel) and atomization (right panel) after the injection [1].

The importance of accurately modelling fuel DHE is well known in IC engine industry [2,3]. The conventional hydrodynamic approach assumed that the concentration of fuel vapour near the droplet surface is maintained at a saturation level, and this approach is universally utilised in computational fluid dynamics (CFD) and heat/mass communities. However, it should be pointed out that the kinetic effect on the droplet evaporation is always noticeable, despite the fact that this evaporation takes place at rather high pressures and temperatures (up to 30 bar and 1,000 K) [4]. The kinetic effect becomes more pronounced for smaller droplets (i.e., radius of droplet $R_0 \leq 5\mu$m) than for larger ones (i.e., $R_0 \leq 20\mu$m). For example, when the droplet's radius is smaller than 5μm at high ambient gas temperatures and pressures such as 1,000 K and 30 bar, the kinetic effect is noticeable in the vicinity of the droplet surface. Preliminary comparisons between the predictions of the simplified kinetic model and the hydrodynamic approach for the typical fuel DHE under IC engine conditions (gas pressure up to 30 bar) showed that the hydrodynamic approach underestimated the droplet lifetime by about $5-10\%$ [4], which led to a corresponding ignition delay and consequently the combustion phasing in IC engines [5,6]. This is likely to compromise the applicability of currently available CFD solvers as predictive tools. Moreover, in extreme cases the injected fuel is typically at transcritical or supercritical state during the injection, mixing and vaporization processes (see Figure 1). Unfortunately, these processes of hydrocarbon fuels into a supercritical environment are not yet well understood. They address the limitations of the current hydrodynamic approach to accurately modelling the fuel DHE.

The hydrocarbon fuel (i.e., dodecane) droplet heating and evaporation ($C_{12}H_{26}$-DHE) under IC engine conditions is a multi-physics, multi-scale, and multi-phase phenomenon, as shown in Figure 2. The liquid fuel and the bulk of its vapour are divided by a Knudsen layer (KL), which represents the kinetic effect taking place in small droplets (i.e., $R_0 \lessapprox 5\mu$m) and is solved by the gas kinetic theory. Its thickness is about several to hundred mean free paths (MFP) of fuel vapour molecules depending on the evaporation rate. The liquid-vapour (LV) interface is sandwiched by KL and the liquid phase and is investigated by molecular dynamics (MD) simulations because of its thickness being at the order of molecular diameter of dodecane, i.e., $\sim$ nanometres. Theoretically, the hydrodynamic approach is still valid in the bulk of both liquid and vapour except both the micro (i.e., KL) and nanoscale (i.e., LV interface) regions. This review will establish a new basis to multi-scale modelling of $C_{12}H_{26}$-DHE under IC engine conditions. Therefore, it is strongly recommended that the kinetic effects should be considered when modelling the evaporation process of small fuel droplets in realistic IC engines. This leads to the introduction of the concept of KL (see Figure 2), which separates the liquid surface from the bulk of the vapour.

Preprints (www.preprints.org) | NOT PEER-REVIEWED | Posted: 8 April 2022 doi:10.20944/preprints202204.0067.v1

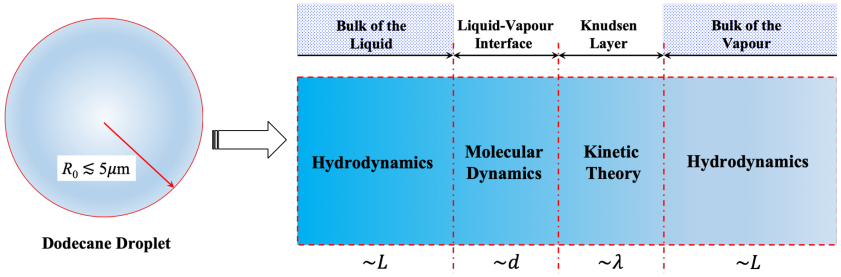

Figure 2. Multi-scale modelling of the hydrocarbon fuel (dodecane) droplet heating and evaporation ($C_{12}H_{26}$-DHE) under IC engine conditions to account for the kinetic effect. The liquid-vapour (LV) interface is sandwiched by Knudsen layer (KL) and the liquid phase, and KL separates the liquid surface from the bulk of the vapour. The radius of the fuel droplet R_0 is specified as the characteristic length L, λ is the mean free paths (MFP) of fuel vapour molecules, and d is the molecular diameter of dodecane.

There are two major flaws in the previous kinetic methods. First, ignoring the inelastic collisions is only justified for mono-atomic molecules, but it appears to be inaccurate in the case of such complex molecules as fuels (approximated by dodecane). Moreover, it seems to be no reason to ignore their contributions if the number of internal degrees of freedom of dodecane molecules exceeds one hundred [7]. Second, the LV interface separating the liquid and vapour phases is assumed to be infinitely thin and taken as a thickness of zero [8], which results in the absence of the kinetic boundary condition (KBC) for solving the Boltzmann transport equation in the vicinity of droplet surface, i.e., KL. To make well-informed predictions of the injection process and a smart ignition for combustion phasing, multi-scale modelling of $C_{12}H_{26}$-DHE is desirable.

The practical implementation of the kinetic effects, however, requires the specification of boundary conditions at the LV interface and the interface between the kinetic and hydrodynamic regions (see Figure 2). Furthermore, the evaporation coefficient of the fuel droplet was taken assumed values [4], which were derived from water droplets [9]. Alternatively, it was assumed that this coefficient is equal to 1 [10,11]. The rigorous justification of the KBC at the LV interface needs to be based on MD simulations [12,13], which is an appropriate scientific tool for obtaining molecularly accurate dynamic information at micro and nanoscales (the magnitude of LV interface thickness). The MD simulations enable us to explore the mechanism of chain-like molecules ($C_{12}H_{26}$) evaporating into the background gas (approximated by N_2) under various temperatures and pressures, i.e., IC engine-like conditions, aiming to formulate a novel KBC for kinetic theory modelling of non-equilibrium gas flows near to the fuel droplet surface.

This review will be focused on the numerical analysis of hydrocarbon fuel (dodecane) droplet heating and evaporation ($C_{12}H_{26}$-DHE) across the different scales, suitable for practical engineering applications. It is anticipated that meeting these objectives will lead to a *multi-physics*, *multi-scale*, and *multi-phase* investigation of $C_{12}H_{26}$-DHE under IC engine conditions. Next section will present the methodologies used to implement the multi-scale modelling of $C_{12}H_{26}$-DHE. Sec. 3 will illustrate the mathematical models developed in each approach crossing each scale, including MD at the LV interface in Sec. 3.1, kinetic theory modelling of KL in Sec. 3.3, and CFD solvers for bulk regions of the fuel liquid and vapour in Sec. 3.4. The surface temperature of droplet and its evaporation time under IC conditions are also estimated in terms of the basis of multi-scale modelling. Conclusions are drawn in Sec. 4.

2. Multi-scale Modelling of Droplet

2.1. Time and Length Scales in Numerical Methods

The time and length scales that are widely used in computational methods are presented in Figure 3. Based on the length and time scales shown in Fig. 3, the numerical models are approximately classified into four categories: Macroscopic (i.e., the Navier-

Preprints (www.preprints.org) | NOT PEER-REVIEWED | Posted: 8 April 2022 doi:10.20944/preprints202204.0067.v1

Stokes-Fourier equations), Mesoscopic (i.e., the Boltzmann equations), Micro/Nano scales (i.e., MD simulations), and Quantum mechanics (i.e., the first principles). These computational methods are also used in heat conduction in micro/nanoscale materials [14]. Different methods are used to handle specific fluid dynamics and heat/mass transfer problems of different range of scales. Although an impressive progress has been made in multi-scale simulations [], a universal solver is still lacking to deal with fluid dynamics or gas dynamics at any scale. Next, we will give a brief to each approach and introduce their applications.

Macroscopic scale Large scale of flow phenomena refer to as the size of vehicles, aircraft and ships in our life, which is visible to the naked eyes. Commercial CFD software such as ANSYS Fluent and open-source codes such as OpenFOAM are commonly used to solve the macroscopic problems in engineering and industry. More complex flows are numerically solved by the turbulence models: Reynolds Averaged Navier-Stokes (RANS) [15], large eddy simulations (LES) [16], and direct numerical simulations (DNS) [17]. For example, the hydrodynamics of submerged flexible vegetation with or without foliage was investigated by using a 3D LES model indicating the decrease of both the vegetation-induced flow resistance force and the vertical Reynolds shear stress [18].

Mesoscopic scale Inbetween the macro and micro/nano scales lies the mesoscopic phenomenon, which involves the Boltzmann transport equations such as kinetic models of gas dynamics at the non-equilibrium state [19]. Besides, the lattice Boltzmann method (LBM) has been emerged as a powerful solver with high parallel computing efficiency in CFD, multi-phase flow and heat transfer communities. For example, the natural convection of solutions under the micro-gravity field [20] and the heat enhancement of power-law fluids in the presence of wall vibrations were investigated by a thermal LBM [21]. Based on the phase-field theory, a two-phase LBM was proposed to capture the migration of supercritical CO_2 in sandstones under conditions of saline aquifers with applications to the carbon capture and storage (CCS) [22]. There are other LBM-based solvers, i.e., the wind analysis simulation with SimScale, and LBSolver/ProLB which allows engineers to accurately simulate transient aerodynamics and aeroacoustics.

Micro/nano scale Diameter of the macro molecules such as polymers and dimensions of highly confined geometries such as a tight pathway of the shale gas [23] can be down to several micrometres and even nanometres. Examples include the micro/nanochannel gas flows with the permeable walls [24,25], the surface acoustic wave (SAW) induced fast flow in nanochannels [26] and the effective viscosity of nanofluidics [27]. Most of the micro gas-flow and nano liquid-flow are based on MD simulations. One of the most popular open-source codes to perform MD simulations is LAMMPS (Large-scale Atomic/Molecular Massively Parallel Simulator (https://www.lammps.org/)). There are other molecular simulation packages such as DL_POLY developed by CCP5 (Computational Collaboration Project 5 - simulation of condensed matter (www.ccp5.ac.uk)) and in-house codes of MD simulations released by The Art of Molecular Dynamics Simulations [28]. In addition to the micro/nano scale fluid flows, the heat conduction in micro/nano devices such as the thermal management also falls into this category [14].

Quantum mechanics refers to an approach to numerically solve Schrodinger equation. We only focus on the first-principles method [29], which is also known as the *ab initio* method. The first-principles method combined with anharmonic lattice dynamics is a very accurate method to predict the thermal conductivity of materials such as metals without any fitting parameter and non-Fourier phonon heat conduction [30–32]. There are first-principles simulation tools such as VASP and Quantum Espresso. The commonly used computational methods for heat conduction and their scope of application were summarised in Ref. [14].

Preprints (www.preprints.org) | NOT PEER-REVIEWED | Posted: 8 April 2022 doi:10.20944/preprints202204.0067.v1

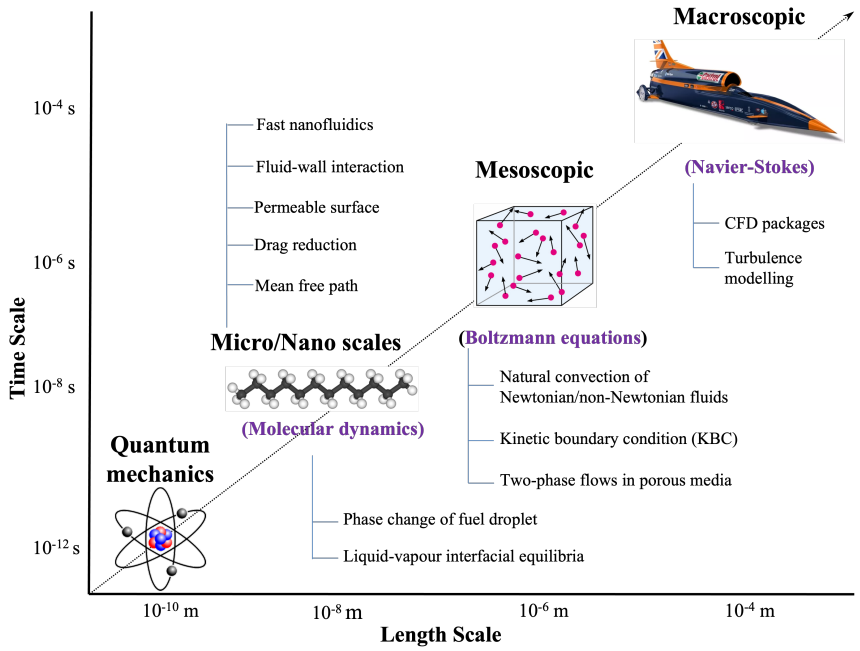

Figure 3. Schematic presentation of time and length scales in computational methods.

This review has threefold to accessing the nano/micro, meso and macroscopic fluid elements across the different scales in DHE under IC engines conditions. Firstly, an MD algorithm for the simulation of hydrocarbon fuel molecules (i.e., dodecane), with emphasis on the evaporation/condensation process at the LV interface, will be introduced. Secondly, a kinetic theory modelling of the non-equilibrium gas flow near to the fuel droplet surface (i.e., KL), which is based on the Boltzmann equations considering the inelastic collision between fuel molecules, will be presented. The evaporation coefficient of evaporating fuel molecules and their velocity distributions at the LV interface obtained in MD simulations are applied to formulate a novel KBC which is used to solve the gas transport equations. Thirdly, the surface temperature of fuel droplet and its evaporation time can be accurately estimated by implementing the kinetic effects into the DHE.

2.2. Molecular Dynamics (MD) Study on Evaporation and Condensation

As mentioned in Sec. 1, rigorous estimation of the evaporation and condensation coefficients requires the application of MD technique [33–36]. One of the most advanced MD investigations of these coefficients for water was reported in Ref.[9]. In that paper, two models for intermolecular potential were used: the Carravetta and Clementi model [37] and the extended simple point charge model [38]. The intermolecular interactions were treated as a combination of the short-range pairwise potential of atoms and the long-range Coulombic interaction in both models. The predictions of the extended simple point charge model reached better agreement with the experimental data than those of the Carravetta and Clementi model. It was also pointed out that the translational motion is of primary importance for the evaporation/condensation process, whereas the effect of rotational motion can be ignored.

A number of models were developed to describe the dynamics of complex hydrocarbon molecules such as dodecane ($C_{12}H_{26}$), including the Optimized Potential for Liquid Simulation (OPLS) [39–42]. These models were reviewed in Ref. [43] and they also suggested their new model. The new model was based on the OPLS potentials but claimed higher accuracy than the previous models. All these models are based on the observation that the C-H bond in complex hydrocarbon molecules is much shorter and much stronger than the C-C bond, and also stronger than the van der Waals forces

Preprints (www.preprints.org) | NOT PEER-REVIEWED | Posted: 8 April 2022 doi:10.20944/preprints202204.0067.v1

between dodecane molecules. Thus, both methyl (CH_3) and methylene (CH_2) groups can be regarded as separate atom-like structures in a relatively simple united atom model (UAM) [44]. The underlying physics of all these models is essentially the same, but they differ from the energy parameters and diameters of CH_3 and CH_2 groups, and bond bending and torsion potentials. Ref. [43] applied all the above-mentioned models to complex hydrocarbons to determine their vapour-liquid coexistence curves using the Gibbs-ensemble technique and the configuration-bias Monte Carlo (MC) method. All models gave almost the identical results at standard conditions, but the predicted critical temperatures differed by up to 100 K. It was also claimed that the new model better described the phase change of the vapour-liquid coexistence curve over a large temperature range [43]. Furthermore, Ref. [44] applied the Toxvaerd model [41,42] to the MD simulation of n-octane. Previous MD simulations of n-alkane LV interfaces were focused on interfacial properties, such as phase equilibria, interface tension and thermodynamic parameters [45–49]. However, none of these studies carried on the MD analysis of the vapour-liquid phase equilibria of dodecane ($C_{12}H_{26}$) and the estimation of its evaporation/condensation coefficient.

Besides, the MD simulation of n-dodecane ($C_{12}H_{26}$) in an equilibrium system was performed using AMBER version 10.0 (a package of molecular simulation programme) [50], where a general Amber force field (GAFF) was applied and the potential energy was presented as a sum of bending, torsion, van der Waals and Coulomb energies. As the AMBER takes the hydrogen atoms explicitly into account, it can be called all atoms model (AAM). Due to the increased number of interactions calculated, this AAM is much more time-consuming compared to UAM. Hence, the UAM model is more attractive in practical engineering applications. Moreover, the UAM was successfully used for modelling the phase behaviour of a large number of n-alkanes ranging from pentane (C_5H_{12}) to octatetracontane ($C_{48}H_{98}$) [43].

In Sec. 3.1, the OPLS potential will be chosen to study the phase transition of dodecane droplet including the vapour-liquid coexistence, the interface thickness, and the evaporation/condensation coefficient over a wide range of liquid temperature.

2.3. Kinetic Boundary Condition (KBC)

As discussed in Sec. 1, the practical application of the combined or kinetic modelling requires the specification of boundary conditions at the droplet surface and at the interface between the kinetic and hydrodynamic regions. These boundary conditions include the evaporation/condensation coefficient at the droplet surface and the velocity distribution function (VDF) of molecules leaving the droplet surface or entering the kinetic region from the hydrodynamic region. It was implicitly or explicitly assumed that this distribution function is isotropic Maxwellian in both cases [4,10,11,51,52]. The values of the evaporation/condensation coefficient were also assumed equal to 0.04 and 0.5 (the minimal and average value of this parameter of water) [4] or unity [10,11,51,53]. None of these assumptions was rigorously justified. The only practical way to perform this justification is to carry on the MD simulations in the vicinity of fuel droplet surface, i.e., the LV interface.

The LV interface between the gas and liquid is typically a couple of molecular diameters wide [12]. Hence, MD simulation is ideally suited to probe the molecular mechanism of phase change. Ref. [54] used MD to simulate the stationary evaporation and condensation between two liquid slabs kept at different temperatures and calculated the evaporation and condensation coefficients for an argon-like fluid. Ref. [55] simulated the evaporation into vacuum by removing all molecules that left the gas region of the simulation cell with a completely absorbing wall and found the evaporation/condensation coefficient for simple liquids in a wide range of temperatures. In addition, Refs. [56] and [57] obtained the condensation coefficients of argon and water in MD simulations. We aim to further investigate the evaporation and condensation processes of fuel droplet (i.e., dodecane) with particular emphasis on the determination

Preprints (www.preprints.org) | NOT PEER-REVIEWED | Posted: 8 April 2022 doi:10.20944/preprints202204.0067.v1

of evaporation/condensation coefficient and the illustration of VDF in various locations relative to the LV interface, which will be presented in Sec. 3.2.

In kinetic theory, the LV interface is modelled as a surface of zero thickness [4,10] and molecules hitting it from the vapour phase are condensed or reflected. Using MD simulations for relatively simple molecules, it had been found that the condensation probability is independent on the incoming velocity [9,54]. Moreover, the incident angle of the molecules had no noticeable effect on the condensation coefficient [9]. The VDF of molecules leaving the interface from the liquid phase f^{out} is usually presented as a sum of the distribution functions of the evaporated part σf^e and the reflected part $(1-\sigma)f^r$ [58]:

$$f^{out} = \sigma f^e + (1-\sigma)f^r, \tag{1}$$

where σ is the evaporation/condensation coefficient, f^e is the distribution function of vapour molecules at the temperature of liquid, and v_x is the velocity component normal to the interface. For evaporated molecules, it is typically assumed that their distribution function is isotropic Maxwellian with the temperature of liquid without a drift velocity [59]. The isotropic Maxwellian distributions with drift velocities were also reported [54,60].

Eq. (1) is called the kinetic boundary condition (KBC) in kinetic theory modelling [10,11]. Alternative formulations of KBC were discussed in Refs. [8,54,60,61]. Previous studies of $C_{12}H_{26}$-DHE under IC engine conditions used the KBC of Eq. (1) with the evaporation/condensation coefficient set to unity and assuming that the VDF was isotropic Maxwellian [10,11,51,52]. In addition, Eq. (1) was used for monatomic molecules (i.e., argon) [62] and polyatomic molecules (i.e., water and methanol) [63] in MD simulations.

The maximum mass flux density of the molecules evaporated from the liquid surface, assuming that f^e is isotropic Maxwellian, is given by the Hertz formula [64]:

$$j_m = \rho_v \sqrt{\frac{k_B T_l}{2\pi m}}, \tag{2}$$

where ρ_v is the density of saturated vapour in equilibrium state at the liquid temperature T_l, m is the molecular mass, and k_B is the Boltzmann constant. The ratio of the actual mass flux density of the evaporated molecules j_e to its maximum value j_m is defined as the evaporation coefficient σ_e. The condensation coefficient is defined as the ratio of the actual mass flux of condensed molecules j_c to j_m. Under the equilibrium condition, the condensed mass flux should be equal to the evaporated mass flux, i.e., $j_c = j_e$, which implies that $\sigma_c = \sigma_e$. The condensed mass flux j_c and the evaporated mass flux j_e can be calculated by counting the number of molecules crossing a unit area per unit time at the interface zone. In this review, we choose the evaporation coefficient in our discussions.

2.4. Kinetic Formulation of Evaporation and Condensation

The kinetic analysis of gas dynamics needs to be based on the solution to the Boltzmann equation, which considers the collision process. Note that the Boltzmann equation itself approximates the more general chain of Bogolubov-Born-Green-Kirkwood-Yvon (BBGKY) chain of equations [10,65].

A number of approximate solutions to the Boltzmann equation were suggested. One of them was based on the replacement of this equation by the system of equations for the moments of the distribution function [66]. Although the replacement was important from the point of view of theoretical developments, it had limitations in practical applications to non-stationary and multi-dimensional problems. An alternative approximation is widely known as the method of the model kinetic equations. In this method, the actual collision integral is not calculated but modelled. One of the most widely used variations of this method was suggested in Ref. [67] and known as Bhatnagar-Gross-Krook (BGK) method [68,69]. More advanced versions of the method of the model kinetic equations

Preprints (www.preprints.org) | NOT PEER-REVIEWED | Posted: 8 April 2022 doi:10.20944/preprints202204.0067.v1

were suggested in Ref. [70]. These methods are computationally economical but their accuracy becomes poor when the distribution of gas molecules or ions/electrons deviates considerably from the equilibrium distribution. A more detailed analysis of these approximate methods and the results of their applications were reviewed in a number of monographs and papers [4,71,72]. Although these solutions had been proven useful in qualitative analysis of phenomena and understanding of the underlying physics, their limitations for the quantitative analysis were well known.

It seems that the only way to perform the quantitative analysis of gas dynamics in a general case should be based on the direct numerical methods [73,74]. For non-ionised gases such methods were developed [75,76]. Bird based his approach on direct statistical analyses of the dynamics of individual atoms while Aristov and Tcheremissine developed a new method of the direct numerical solution to the Boltzmann equation. These methods were further developed and applied to the analysis of gas dynamics, including evaporation and condensation problems [76–88]. Attempts to apply these methods to binary mixtures were also reported [82–87]. Numerical difficulties in the analysis of these mixtures, however, imposed a number of restrictions on the properties of molecules: molecules were assumed to be mechanically identical [82,85,86]; the difference in the masses of molecules was considered, but their diameters were assumed to be the same [83,86]. These assumptions can hardly be justified in many practical engineering applications, where molecules in binary mixtures have very different diameters, such as the problem of evaporation of heavy hydrocarbons (i.e., dodecane) into air (i.e., nitrogen).

In addition, the contribution of inelastic collision was ignored in the above-mentioned models. This assumption could be justified in the case of monoatomic molecules, but appears to be highly questionable in the case of such complex molecules as dodecane ($C_{12}H_{26}$). Even if the analysis of the dynamics of these molecules is simplified by considering the UAM [12], the number of its internal degrees of freedom is expected to exceed one hundred. There seems to be no justification for ignoring the inelastic collisions.

Perhaps the first phenomenological model for the binary collisions in a gas mixture having continuous internal energy was developed in Ref. [89]. This model was applied to Monte Carlo (MC) simulation of rarefied gas flows. Since the publication of this pioneering paper, a substantial number of papers had been published, in which various models of inelastic collision were introduced [90–101]. Based on the Wang-Chang and Uhlenbeck results for polyatomic gases [102], Ref. [103] introduced a kinetic model for gases with the internal degrees of freedom, which is, as in the case of the BGK model, related to the Boltzmann collision integral. Moreover, Ref. [104] proposed another solution of Wang-Chang-Uhlenbeck master equation to deal with the non-equilibrium processes in a gas with the internal degrees of freedom by generalising the Boltzmann equation. Also, Ref. [105] used the Borgnakke-Larsen collision model to deal with the steady condensation of a polyatomic gas, and a simpler BGK-type collision model was proposed for the steady evaporation [106,107].

In Sec. 3.3, a typical kinetic theory modelling considering the inelastic collision between fuel molecules (i.e., dodecane) will be introduced, and its numerical solution is also presented.

2.5. Convectional Fluid Dynamics of Droplet

As shown in Figure 2, two regions of gas above the surface of evaporating fuel droplet are considered: Knudsen layer (KL) and the vapour fuel region. In contrast to Refs. [4,10,11,51,52], we relax the assumption that the liquid thermal conductivity is infinitely large and consider the processes in the liquid phase region as well. All three regions (i.e., the liquid and vapour bulk regions, and KL) are schematically shown in Figure 2. As in Refs. [10,11,51,52], we assume that the gas consists of two components, i.e., the fuel vapour and a background air, both in KL and the vapour region. It is assumed that the contribution of chemical reactions of fuel vapour and oxygen can be

Preprints (www.preprints.org) | NOT PEER-REVIEWED | Posted: 8 April 2022 doi:10.20944/preprints202204.0067.v1

ignored. Fuel vapour and air dynamics in KL are described by the Boltzmann equations, while the conventional hydrodynamic analysis (i.e., the Navier-Stokes-Fourier (NSF) equations) is applied to the bulk liquid and vapour regions. The numerical models used in all three scales (i.e., LV, KL and the bulk) and the conditions at the interface between the regions will be discussed in Sec. 3.4.

2.6. Multi-scale Universal Interface (MUI)

For the dynamic process of DHE, i.e., moving interfaces across the different scales, it is recommended to use a domain-decomposed method (DDM) to simultaneously couple the classical MD and CFD solver by matching the state variables and/or fluxes across the hybrid interface. DDM, which was originally from the Schwarz alternating method to solve the elliptic partial different equations (PDEs), is largely and successfully extended and proved to play a big role in multi-scale modelling of complex fluids and materials in terms of computational efficiency and physical accuracy. For simple fluids, a continuum perspective has been taken to couple the MD and NS equations by matching the state variables and/or fluxes across the hybrid interface. For complex fluids such as a dodecane droplet, the complex structure of the molecules is represented by a discrete perspective and the MD has been coupled with the coarse-grained MD (CGMD) in terms of the interpolation of forces between the two levels of descriptions [108].

This approach utilises an MPI-based general coupling library, i.e., a multi-scale universal interface (MUI) [109], which enables us to make a coupling effort in a wide range of multi-scale simulations. Our aim is to perform the complex multi-scale simulations involving nano/micro, meso and macroscopic elements in DHE problems. The library introduces a data sampler concept, which is combined with a hybrid dynamic/static typing mechanism to create an easily customisable framework for solver-independent data interpretation. The library integrates the MPI MPMD support and an asynchronous communication protocol to handle the inter-solver information exchange regardless of the solvers' own MPI features. Particularly, the template meta-programming is massively employed to simultaneously reduce the computing costs and make the coding friendly. For example, Bian *et al* considered the conjugate heat transfer between a solid domain and a fluid domain by coupling the particle-based energy-conserving dissipative particle dynamics (eDPD) method with the finite element method (FEM) [108]. It also demonstrated the flexibility of the framework in handling the heterogeneous models and solvers. More implements of the MUI library into the hybrid algorithm and multi-scale modelling can be found in its applications to soft matters.

3. Mathematical Models

Based on the multi-scale presentation of fuel DHE, each approach at different scales will be introduced with the increasing of scales, i.e., MD simulations at the LV interface ($\sim$ nano scale), kinetic theory modelling in KL ($\sim$ micro scale), and hydrodynamics in bulk regions ($\sim$ macroscopic scale).

3.1. Liquid-Vapour (LV) Interfacial Dynamics

3.1.1. Intermolecular potentials in MD

We take the dodecane as an example, and the interactions (i.e., the primary forces) between fuel molecules that are presented in Figure 4 include the bond-angle bending and the dihedral angle torsion within one molecule.

Preprints (www.preprints.org) | NOT PEER-REVIEWED | Posted: 8 April 2022 doi:10.20944/preprints202204.0067.v1

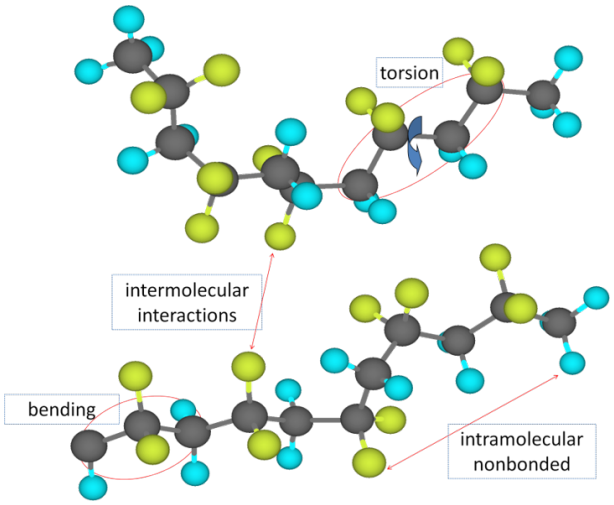

Figure 4. Schematic presentation of the molecular interactions: the bond-angle bending and the dihedral angle torsion within one molecule.

The MD simulation of dodecane droplet in this review is based on UAM, and the representation of UAM applied to a dodecane molecule is schematically illustrated in Figure 5.

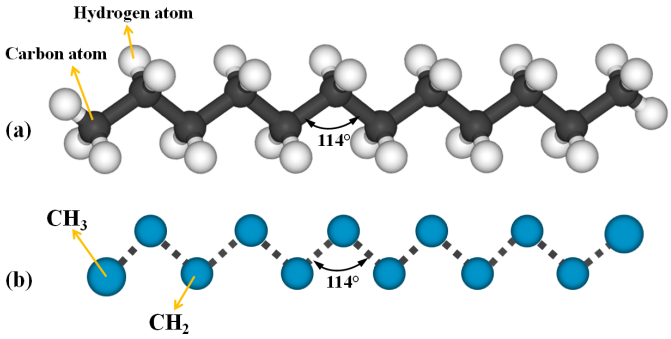

Figure 5. Schematic presentation of molecular structure of dodecane ($C_{12}H_{26}$) (a) and its UAM approximation with methyl (CH_3) and methylene (CH_2) groups (b). The bending angle between neighbouring bonds is 114°. Reproduced from Ref. [13].

As mentioned in Sec. 2.2, the Optimized Potential for Liquid Simulation (OPLS) is used to describe the dynamics of dodecane. First, the non-bonded interactions between atoms, which belong to either different chains or the same chain but more than four atoms apart, are characterised by the truncated Lennard-Jones (L-J) 12-6 potential [28,110]:

$$u^{LJ}(r_{ij}) = 4\varepsilon_{ij}\left[\left(\frac{\sigma_{ij}}{r_{ij}}\right)^{12} - \left(\frac{\sigma_{ij}}{r_{ij}}\right)^{6}\right]. \quad (3)$$

The energy parameters of CH_2 and CH_3 groups are $\varepsilon_{CH_2}/k_B = 47$ K and $\varepsilon_{CH_3}/k_B = 114$ K, respectively. According to the geometric rule, the energy parameter between CH_2 and CH_3 groups is estimated as $\varepsilon_{CH_2-CH_3}/k_B = \sqrt{\varepsilon_{CH_2}\varepsilon_{CH_3}}/k_B = 73.2$ K. The diameters of CH_2 and CH_3 groups are assumed to be equal and estimated as $\sigma_{ij} = 3.93$ Å. The L-J 12-6 interaction is truncated at 13.8 Å in MD simulations.

Preprints (www.preprints.org) | NOT PEER-REVIEWED | Posted: 8 April 2022 doi:10.20944/preprints202204.0067.v1

Second, the interactions within the chains include bond bending and torsion with the bond length constrained at 1.53 Å. The bending can take place between any three neighbouring atoms and the potential is [111]:

$$u^{bend}(\theta) = \frac{1}{2}k_\theta(\theta - \theta_0)^2, \tag{4}$$

where the bending coefficient is estimated as $k_\theta/k_B = 62,500$ K/rad^2, and the equilibrium angle is $\theta_0 = 114^\circ$(see Figure 5).

Third, the torsion can take place between four neighbouring CH_3 and/or CH_2 groups (see Figure 2 of Ref. [12]) and the torsion potential is applied to [39]:

$$u^{tors}(\Phi) = c_0 + 0.5c_1(1 + \cos\Phi) + 0.5c_2(1 - \cos 2\Phi) + 0.5c_3(1 + \cos 3\Phi), \tag{5}$$

where the coefficients $c_0/k_B = 0$ K, $c_1/k_B = 355$ K, $c_2/k_B = -68.19$ K, $c_3/k_B = 791.3$ K, and Φ is the torsion dihedral angle. The equilibrium value of Φ is 180°.

3.1.2. Equilibrium simulation of a vapour-liquid coexisting system

Based on OPLS, we considered two nanodroplets consisting of 400 [12] and 720 [112] dodecane ($C_{12}H_{26}$) molecules, respectively. These molecules were initially oriented along the x-axis and placed at the centre of the simulation box illustrating the zigzag configurations, as shown in Figure 5 (b). The number of molecules in each direction was chosen based on the number density of droplet molecules correspondingly.

The equations of motion of the united atoms (i.e., CH_3 and CH_2 groups) were integrated using the Verlet leapfrog method [28,110]. For the chain-like molecules of dodecane, the bond length constraint was applied to the neighbouring atoms only, and the bond length was also constrained by the SHAKE scheme adjusting the atom coordinates one by one cyclically to satisfy a given tolerance [28,110,113]. Periodic boundary conditions were applied in all directions. To achieve a higher calculation efficiency, the reduced units were used for the physical parameters [110]. Other thermodynamic parameters were reported in Ref. [33]. A general expression of the numerical algorithm for MD simulations is summarised in Figure 6.

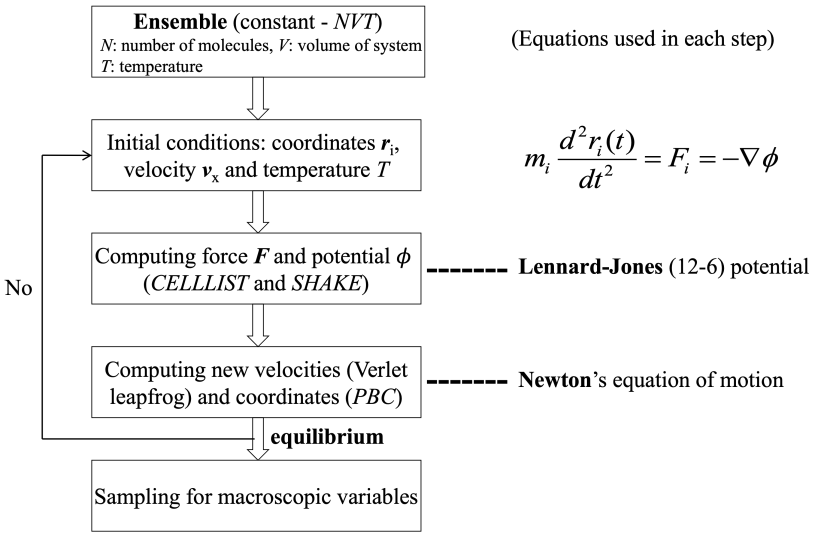

Figure 6. MD algorithm in a constant-NVT ensemble.

The vapour-liquid coexistence curve for temperatures ranging from 400 to 550 K is shown in Figure 7, based on the equilibrium systems of simulations using 720 molecules. It indicates that the density of the liquid phase decreases with the increasing of the liquid temperature, and MD results reach good agreement with both experimental [114] and MC data [43].

Preprints (www.preprints.org) | NOT PEER-REVIEWED | Posted: 8 April 2022 doi:10.20944/preprints202204.0067.v1

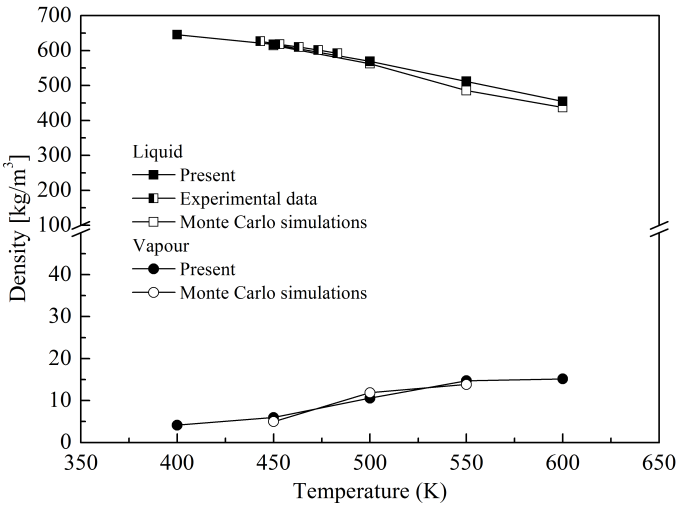

Figure 7. Vapour-liquid coexistence curves in the equilibrium state as predicted by MD simulations compared to experimental [114] and MC data [43]. Reproduced from Ref. [12].

The thickness of the transition layer (i.e., the LV interface) is defined as the thickness of the region where the bulk vapour phase changes to the bulk liquid phase. This refers to the thickness over which the density of dodecane changes from $0.95\rho_l$ to $(\rho_v + 0.01\rho_l)$, where ρ_l and ρ_v are densities of liquid and vapour, respectively. It was found that the thickness of the transition layer of dodecane ranges from 2.3 to 3.5 nm when the temperature increased from 400 K to 550 K. These values are noticeably larger than those of argon [9], water [9] and methanol [63]. The larger thickness of the transition layer at high temperatures may reduce the evaporation/condensation probability of dodecane molecules at the liquid surface. For chain-like dodecane molecules, the thick transition layer would act as a barrier to the condensation of vapour molecules or the evaporation of molecules leaving the liquid surface. Hence, it is expected that the increased thickness of the transition layer at high temperatures would result in smaller evaporation/condensation coefficients. This will be verified by the MD estimation of the evaporation/condensation coefficient in Sec. 3.1.3.

In addition, it was found [12] that the chains lie preferentially at the LV interface, but not completely, parallel to the interface, which is consistent with the results obtained for other polymer or n-alkane chains [46,53,115,116]. This orientation restricts the rotation of molecules in the immediate vicinity of the interface, which is consistent with the observation that the translation of the chains contributes more to evaporation than their rotation does [12].

Based on the evaporation and condensation behaviours of dodecane [13], trapping-desorption evaporation/condensation had never been reported for simple molecules. In these cases, the chain-like dodecane molecules were trapped at the LV interface for a short period. The effect of the translational energy on the evaporation and condensation processes of n-dodecane is similar to its effect on the monatomic molecule of argon [54] and polyatomic molecules of water and methanol [56]. This supports the idea of activation energy in the transition layer, which follows from the transition state theory [56]. The transition layer builds a three dimensional structure at the LV interface with a kind of interfacial resistance. The fact that the molecules in the transition layer preferentially lie parallel to the interface is expected to contribute to the blocking of molecular evaporation and condensation.

3.1.3. Evaporation coefficient

As mentioned in Sec. 1, the evaporation coefficient of dodecane took the minimal and average values of this coefficient for water, 0.04 and 0.5, or 1 in the previous work. The measurements and estimations of this coefficient for water were reviewed in

Preprints (www.preprints.org) | NOT PEER-REVIEWED | Posted: 8 April 2022 doi:10.20944/preprints202204.0067.v1

Ref. [117]. None of these values can be rigorously justified. Although the results of the previous work enable us to illustrate the kinetic effects on the evaporation processes in diesel fuel, but we still are unable to use these models as a predictive tool for engineering applications. Rigorous estimation of the evaporation coefficient should be based on the MD simulation [33–36]. MD simulations is an appropriate scientific tool for obtaining molecularly accurate dynamic information at micro and nanoscales (the magnitude of LV interface thickness). Alternatively, the transition state theory (TST) was suggested to evaluate the evaporation coefficient for various substances [56]. Based on TST, the evaporation process at the LV interface is considered as a kind of chemical reaction and the general theory of rate process is applied [118]. As a result, the average evaporation coefficient can be expressed by:

$$\overline{\sigma} = \left[1 - \left(\frac{V^l}{V^g}\right)^{1/3}\right] \exp\left[-\frac{1}{2}\frac{1}{\left(\frac{V^g}{V^l}\right)^{1/3} - 1}\right], \tag{6}$$

where V^l and V^g are specific volumes of liquid and gas, respectively. The predicted value of $\overline{\sigma}$ in Eq. (6) is dependent on the surface temperature of droplet. It is close to one at the triple point and decreases to zero at the critical point. The evaporation coefficient in Eq. (6) was shown to be in good agreement with the MD results of argon [54,56], water [9] and methanol [57,63]. It is not clear, however, whether this approach can be applied to complex chain-like molecules such as dodecane ($C_{12}H_{26}$). The TST does not consider the detailed molecular structure and non-translational motion in chain-like molecules and complex evaporation/condensation behaviours such as trapping and desorption. The application of Eq. (6) to dodecane needs more rigorous justification, i.e., based on MD simulations. Thus, the evaporation/condensation coefficient will be investigated at the LV interface using MD simulations.

The molecular mechanism of droplet evaporation and condensation at the LV interface is shown in Figure 8. Assuming that the distribution function of molecules at the interface is isotropic Maxwellian, the maximum flux by Eq. (2) can be justified. Hence, the evaporation and condensation coefficients have been estimated as the ratios of evaporated and condensed mass fluxes to the maximum fluxes given by Eq. (2). The results will be compared with the values of coefficient predicted by TST in Eq. (6).

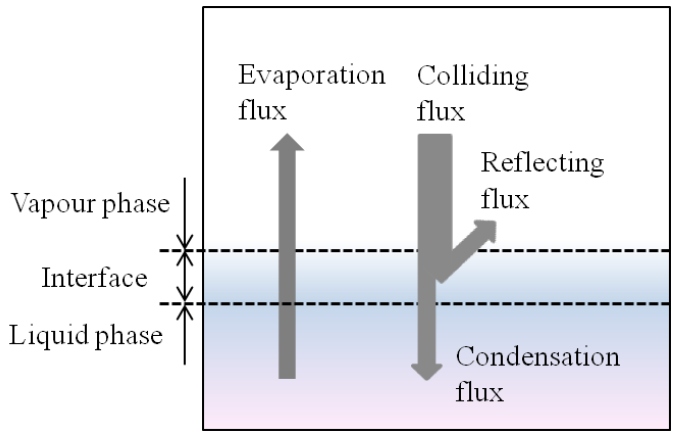

Figure 8. Schematic presentation of the molecular mass flux of evaporation and condensation.

The evaporation coefficient obtained in a droplet consisting of 720 molecules decreases from about 0.93 at 400 K to about 0.45 at 550 K. The densities of the liquid and vapour phases obtained in MD simulations were applied to predict the values of the evaporation coefficient by TST. It indicates a general agreement of the condensation coefficient between MD results and TST predictions [50]. The condensation coefficient of other substances (argon [54,62], water [9,63] and and methanol [63]) in MD simulations

Preprints (www.preprints.org) | NOT PEER-REVIEWED | Posted: 8 April 2022 doi:10.20944/preprints202204.0067.v1

also illustrates that it decreases with the increasing of the liquid temperature regardless of the type of molecules. This is consistent with the results for the LV thickness: the thicker interfaces at higher temperatures are expected to reduce the possibility of the evaporating molecules from the transition layer.

The evaporation coefficient for complex molecules, like dodecane, would be expected to be lower than for simpler molecules due to the constraint imposed by the rotational motion of molecules in the liquid phase [119]. However, it was found in MD simulations that the rotational energy had no noticeable effect on this coefficient and its value was mainly controlled by the translational energy in agreement with the previously reported results [9,12]. On the other hand, based on TST, we can expect that this coefficient is close to unity at low temperatures when $(\frac{V^g}{V^l})^{1/3}$ is large, and decreases with the increasing temperature due to the decrease of the ratio $(\frac{V^g}{V^l})^{1/3}$. This trend is consistent with the prediction of MD simulations. The evaporation coefficient predicted in MD simulations will be used to formulate a novel boundary condition at the interface between fuel liquid and its vapour, instead of previously assumed values of 0.04, 0.5 or 1.0.

3.2. Revised Boundary Conditions

As mentioned in Ref. [13], it is generally assumed that the VDFs of the evaporated molecules and the molecules entering the kinetic region from the vapour phase are isotropic Maxwellian. In what follows the range of applicability of this assumption is based on the calculations of VDF in MD simulations. The MD analysis focuses on the investigation of these distributions in the liquid phase, at the LV interface and in the vapour phase.

Although we appreciate that this result needs to be confirmed by MD simulations with a larger number of molecules, we believe that the traditional approach to the formulation of the boundary conditions in kinetic theory modelling, when the VDF of the evaporated molecules is assumed to be isotropic Maxwellian with the same temperatures for all velocity components, needs to be revisited.

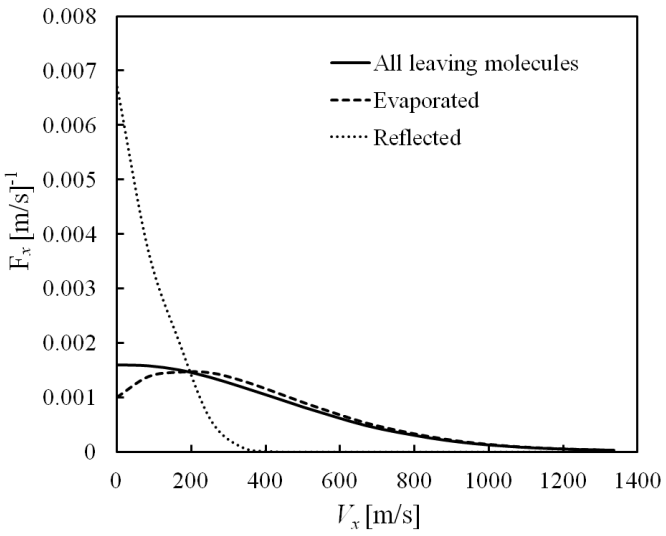

Figure 9. Normalised velocity distributions of evaporated and reflected molecules from the LV interface and sum of all molecules leaving this surface at the liquid temperature of 500 K. Reproduced from Ref. [120].

As can be seen from Figure 9, for the velocity component normal to the interface, v_x, the distribution function for all molecules leaving the surface is close to isotropic Maxwellian, but the distributions for the evaporated and reflected molecules noticeably deviate from the Maxwellian one. The VDF of evaporated molecules is less than that of

Preprints (www.preprints.org) | NOT PEER-REVIEWED | Posted: 8 April 2022 doi:10.20944/preprints202204.0067.v1

the Maxwellian for small velocities but greater than that of the Maxwellian for high velocities. The VDF of reflected molecules, however, is greater than that of the Maxwellian for small velocities but less than that of the Maxwellian for high velocities. Thus, the main contribution to the molecules leaving the droplet surface at small velocities comes from the reflected molecules, while the main contribution to these molecules leaving the droplet surface at high velocities comes from the evaporated molecules.

Moreover, it was found that the VDF of molecules in the liquid phase and at the LV interface had been shown to be close to isotropic Maxwellian with temperatures equal to that of the liquid phase [121]. The VDF of molecules in the vapour phase, however, had been shown to deviate from the classical isotropic Maxwellian distributions. It can be approximated as bi-Maxwellian with temperatures in the direction normal to the LV interface larger than those in the directions parallel to the LV interface. Therefore, the boundary conditions in kinetic theory modelling can be revised in terms of the realistic VDF of the evaporated molecules in the vapour phase approximated as bi-Maxwellian.

3.3. An Inelastic Collision Model

Despite considerable progress in the development of kinetic models of evaporation, these models are still based on a number of assumptions and their applicability to combustion engines is not at first evident. For example, it was assumed that the temperature of the outer boundary of the kinetic region was equal to the droplet surface temperature and the heat transfer process inside this layer was ignored. In addition, the contribution of inelastic collisions to the processes in gases was focused either on the analysis of collisions between inelastic spheres [94,122] or simple diatomic or triatomic molecules [90,123]. The generalisation of these models to complex hydrocarbon molecules was not feasible at that time. Furthermore, the number of internal degrees of freedom of dodecane is expected to exceed one hundred, and there is no justification to ignore their inelastic collisions.

The model proposed in this review is different from those suggested earlier, although it is based on some widely used assumptions. Although this model has been tested for some rather specific problems, it can be applied to any molecules with arbitrary large number of internal degrees of freedom. This model is expected to be effective for the analysis of such complex molecules as dodecane. As in Refs. [10,11,51,52], the molecules were approximated as hard spheres. In contrast to this approximation, we adopt a well-known inelastic hard spheres (IHS) model to take into account the inelastic effects during the collisions of these spheres [98].

The binary collision is still considered between two colliding molecules in this model. Regardless of the nature of the collision between them, their centre of mass is not affected by this collision. The state of the molecules after the collision is described in a reference system linked with this centre of mass. In this reference system, each molecule has three translational and a certain number of internal degrees of freedom, and the total number of degrees of freedom of both molecules is N. During the colliding, energies of each molecule are redistributed among the degrees of freedom, but the total number of degrees of freedom remains unchanged. It is also assumed that none of these degrees of freedom has any preference over the others. This allows us to consider a random redistribution of the total energy among these degrees of freedom during the collision. For each of these degrees of freedom we allocate one dimension in a N-dimensional space describing all degrees of freedom. Once we have done this, we consider a sphere in this space with its centre at the origin where energies of all degrees of freedom are equal to zero and the energy is conserved at the surface of the sphere which is located in the system of reference relative to the centre of mass such as dodecane molecules.

Furthermore, we introduce a N-dimensional vector $\mathbf{X} = (x_1, x_2, \ldots\ldots x_N)$ to represent each degree of freedom in a curvilinear coordination $(\mathbf{e_1}, \mathbf{e_2}, \ldots\ldots \mathbf{e_N})$ under the conditions that the norm of each vector $\mathbf{e_i}$ is equal to one and the component x_i is mutually perpendicular to each other.

Preprints (www.preprints.org) | NOT PEER-REVIEWED | Posted: 8 April 2022 doi:10.20944/preprints202204.0067.v1

The redistribution of energy between the degrees of freedom during the collision process can be described in terms of the rotation of vector $\mathbf{X}$ in the N-dimensional space. Recall that none of the degrees of freedom has any preference over the others this rotation of the vector $\mathbf{X}$ can be considered as random with uniform probability distribution. Based on the conservation of the total energy during the collision, the new position of vector $\mathbf{X}$ after rotation remains at the surface of the sphere with the same radius. It also implies a rotation matrix relative to the redistribution of energies after the collision. The algorithm for the construction of the rotation matrix can be found in Ref. [7].

An example of the temporal evolution of the system with 100 degrees of freedom was investigated in Ref. [7]. The model described above can be generalized to the case when the probabilities of excitation of various degrees of freedom are unequal. This could be achieved by introducing a weighting function and/or activating the range limit of degrees of freedom.

Following Ref.[76], the numerical solution of the Boltzmann equation (for one or several components) is performed in two steps to implement the inelastic collisions between different molecules. Firstly, molecular displacements are calculated without the occurrence of collisions. Secondly, the collision is relaxed under the assumption of spatial homogeneity.

Ignoring the effects of collision, a discretised form of the Boltzmann equation updating molecular displacements for each component is presented as

$$\frac{\Delta f}{\Delta t} + \mathbf{v}\frac{\Delta f}{\Delta \mathbf{r}} = 0, \tag{7}$$

where $f \equiv f(\mathbf{v}, \mathbf{r}, t)$ is the distribution function of velocity $\mathbf{v}$ in physical space $\mathbf{r}$ and at time t.

In an inelastic collision, the total internal energy in each velocity range should be conserved, which implies that

$$\frac{\Delta(E_{\text{int}} f)}{\Delta t} + \mathbf{v}\frac{\Delta(E_{\text{int}} f)}{\Delta \mathbf{r}} = 0, \tag{8}$$

where $E_{\text{int}} \equiv E_{\text{int}}(\mathbf{v}, \mathbf{r}, t)$ are internal energies of molecules with $\mathbf{v}$ at time t and in space $\mathbf{r}$. Based on the splitting finite-difference scheme, a numerical algorithm of the Boltzmann equation is described in Ref. [10].

The inelastic collision model described had been tested in three simple one-dimensional examples [19]: shock wave structure in nitrogen, one-dimensional heat transfer through a mixture of n-dodecane and nitrogen and one-dimensional evaporation of n-dodecane into nitrogen. In the first problem, the predictions of the model, taking into account the contribution of the rotational degrees of freedom, were shown to be close to experimental data and the predictions of the earlier developed inelastic collision model. This problem had been generalized to a hypothetical case when the number of internal degrees of freedom of nitrogen (N_{int}) was assumed to be in the range 0 to 10. It had been shown that the results visibly changed when N_{int} was increased from 0 to 2 but remained practically unchanged at $N_{\text{int}} \geq 6$. The predicted heat flux for the second problem had been shown not to depend on the number of internal degrees of freedom of the mixture N_{int} when this number exceeded about 15. In the third problem, the predicted mass flux of n-dodecane also remained almost unchanged at $N_{\text{int}} \geq 15$. These results shed the light for considering systems with arbitrarily large numbers of internal degrees of freedom by reducing the analysis of these systems to the analysis of systems with relatively small number of internal degrees of freedom.

3.4. Multi-scale Modelling of Droplet

As illustrated in Fig. 2, when the kinetic effect is noticeable in DHE, two regions of gas above the surface of an evaporating droplet should be considered: KL and the

Preprints (www.preprints.org) | NOT PEER-REVIEWED | Posted: 8 April 2022 doi:10.20944/preprints202204.0067.v1

vapour region. In the most comprehensive model, it is assumed that the gases consist of two components, i.e., the fuel vapour and background gas (air), and both mass and heat transfer processes in KL are taken into account [51]. The analysis of these processes in KL is based on the numerical solution of the Boltzmann equations for the fuel vapour and background gas with the relevant boundary conditions.

Ref. [52] suggested simple approximate formulae to describe the temporal evolution of fuel droplet radius (i.e., lifetime) and temperature predicted by the kinetic model. These formulae are valid in a range of gas temperatures relevant to the IC engine conditions and fixed values of the initial droplet radius, or in a range of initial droplet radii relevant to the IC engine conditions and fixed values of the gas temperature. The application of these formulae reduces dramatically the CPU requirements of kinetic modelling, which can potentially open the way to the implementation of the kinetic models into engineering CFD codes designed to model DHE in a realistic engineering environment, including that of IC engines [124,125].

Apart from the vapour region, the previous models assumed that there is no temperature gradient inside the droplet using the conventional hydrodynamic approach [3,126–128]. Furthermore, nobody has considered this effect in conjunction with the kinetic theory modelling and non-unity evaporation coefficient. Sec. 3.1.3 has shown that this coefficient can be well below 1 (close to 0.5) especially when the liquid temperature is close to the critical one [12,112,120].

In this review, we will restrict our analysis of DHE to a stationary droplet and ignore the effects of the moving boundary [129,129,130], the formation of the thermal boundary layer around droplets [131] and the effects of thermal radiation [132].

3.4.1. Liquid region

The models for DHE [127,128] were implicitly based on the assumptions that the evaporation rate of droplets is small and the droplet radius R_d does not change during any time step (although this radius changes from one step to another). This means that the effect of a moving boundary on droplet heating was ignored. This is a well known approach used in all available CFD codes. Two approaches were developed to take into account the changes in droplet radius R_d during the time steps. Firstly, it was assumed that R_d is a linear function of time. Secondly, the evolution of droplet temperature was calculated for an *a priori* fixed function $R_d(t)$ [129,131]. These effects, however, will not be considered in present analysis.

Assuming that the droplet heating process is spherically symmetric, the droplet temperature, $T \equiv T(t, R)$, can be found from the solution to the equation for T in the form [133,134]:

$$\frac{\partial T}{\partial t} = \kappa \left(\frac{\partial^2 T}{\partial R^2} + \frac{2}{R} \frac{\partial T}{\partial R} \right) \tag{9}$$

for $0 \leq t < t_e$, $0 \leq R < R_d(t)$, where κ is the liquid thermal diffusivity, $\kappa = k_l/(c_l \rho_l)$, k_l is the thermal conductivity, c_l is the specific heat capacity, ρ_l is the density, R is the distance from the droplet centre, and t_e is the evaporating time. The effect of thermal radiation is ignored.

Remembering the physical background to the problem, we look for the solution to this equation in the form of a twice continuously differentiable function, $T \equiv T(t, R)$, for $0 \leq t < t_e$, $0 \leq R < R_d(t)$. This solution should satisfy the boundary condition:

$$\left(k_l \frac{\partial T}{\partial R} + hT \right) \Big|_{R=R_d(t)} = hT_g + \rho_l L \dot{R}_{de}(t), \tag{10}$$

T is finite and continuous at $R \to 0$, $T_s = T(R_d(t), t)$ is the droplet surface temperature, L is the latent heat of evaporation, h is the convection heat transfer coefficient, and

Preprints (www.preprints.org) | NOT PEER-REVIEWED | Posted: 8 April 2022 doi:10.20944/preprints202204.0067.v1

$\dot{R}_{de}(t) \leq 0$ is the rate of change of droplet radius due to evaporation. Eq. (10) is the energy balance condition at $R = R_d(t)$. The initial condition is taken in the form:

$$T(t=0) = T_0(R), \tag{11}$$

where $0 \leq R \leq R_{d0} = R_d(t=0)$. In conventional hydrodynamic models, the value of $R_d(t)$ is controlled by the vapour diffusion from the droplet surface and droplet thermal swelling. In the present model, it is controlled by the vapour diffusion from the LV interface between the kinetic and hydrodynamic regions (see Figure 2) and swelling, and can be found as follows [3]:

$$\dot{R}_d \equiv \dot{R}_{de} + \dot{R}_{ds} = -\frac{k_g \ln(1+B_M)}{\rho_l c_{pg} R_d} + \frac{R_{d0}}{\Delta t}\left[\left(\frac{\rho(\overline{T}_0)}{\rho(\overline{T}_1)}\right)^{1/3} - 1\right], \tag{12}$$

where $\dot{R}_{ds}$ is the rate of change of droplet radius due to swelling (or contraction), $B_M = Y_{vRd}/(1-Y_{vRd})$ is the Spalding mass transfer number (assuming that there is no vapour in the ambient gas), Y_{vRd} is the mass fraction of vapour at the LV interface between the kinetic and hydrodynamic regions, which is ultimately controlled by gas temperature T_{Rd} in this region [3], $\overline{T}_0$ and $\overline{T}_1$ are average droplet temperatures at the beginning and the end of the time step Δt, and ρ are the corresponding densities. When deriving Eq. (12), we ignored the difference between R_d and $R_d + \delta_{Rd}$. The validity of this assumption was checked by a direct comparison of the results, taking and not taking into account the effects of the sphericity of droplets for the thickness of the kinetic region equal to 10 MFPs, calculated for pressure equal to 30 bars (diesel engine-like conditions) and temperature equal to the fuel droplet surface temperature [11].

Assuming that R_d is fixed during the time step, the analytical solution to Eq. (9) subject to the above boundary and initial conditions is obtained in the form [135]:

$$T(R) = \frac{1}{R\sqrt{R_d}}\left[\sum_{n=1}^{\infty} \Theta_n(t) \sin\left(\lambda_n \frac{R}{R_d}\right) + \frac{\mu_0(t)}{1+h_0}\frac{R}{R_d}\right], \tag{13}$$

where

$$\Theta_n(t) = \Theta_n(0) \exp\left[-\frac{\kappa\lambda_n^2 t}{R_{d0}^2}\right] + f_n \int_0^t \frac{\mathrm{d}\mu_0(\tau)}{\mathrm{d}\tau} \exp\left[-\frac{\kappa\lambda_n^2 (t-\tau)}{R_{d0}^2}\right] \mathrm{d}\tau, \tag{14}$$

$$\mu_0(t) \equiv R_d^{5/2} \frac{h}{k_l} T_g, \tag{15}$$

$f_n = -\frac{\sin\lambda_n}{||v_n||^2 \lambda_n^2}$, $v_n(\xi) = \sin\lambda_n\xi \qquad (n = 1, 2, ...)$.

$$||\, v_n \,||^2 = \frac{1}{2}\left(1 - \frac{\sin 2\lambda_n}{2\lambda_n}\right) = \frac{1}{2}\left(1 + \frac{h_0}{h_0^2 + \lambda_n^2}\right). \tag{16}$$

$\xi = R/R_d$, λ_n are positive solutions to the equation

$$\lambda \cos\lambda + h_0 \sin\lambda = 0 \tag{17}$$

presented in ascending order,

$$h_0 = \frac{h}{k_l} R_d - 1 \tag{18}$$

is assumed to be constant during the time step,

$$\Theta_n(0) = q_n + \mu_0(0) f_n,$$

Preprints (www.preprints.org) | NOT PEER-REVIEWED | Posted: 8 April 2022 doi:10.20944/preprints202204.0067.v1

$$q_n = \frac{1}{|| v_n ||^2} \int_0^1 R_{d0}^{3/2} \xi T_0(\xi R_{d0}) v_n(\xi) \mathrm{d}\xi. \tag{19}$$

The effect of recirculation inside droplets is taken into account based on the effective thermal conductivity (ETC) model [136], in which the liquid thermal conductivity k_l is replaced by ETC

$$k_{\text{eff}} = \chi k_l, \tag{20}$$

where the coefficient χ is defined as

$$\chi = 1.86 + 0.86 \tanh\left[2.245 \log_{10}\left(\mathrm{Pe}_{d(l)}/30\right)\right], \tag{21}$$

$\mathrm{Pe}_{d(l)} = \mathrm{Re}_{d(l)}\mathrm{Pr}_{(l)}$ is the droplet Peclet number, in which liquid transport properties and the maximum surface velocity inside droplets were used. The latter velocity is calculated [136]:

$$U_s = \frac{1}{32}\Delta U \left(\frac{\mu_g}{\mu_l}\right) \mathrm{Re}_d C_F, \tag{22}$$

where $\Delta U \equiv |U_g - U_d|$ is the relative velocity between the ambient gas and droplet, $\mu_{g(l)}$ is the dynamic viscosity of gas (liquid), Re_d is the droplet Reynolds number based on the droplet diameter, and C_F is the friction drag coefficient estimated as [136]:

$$C_F = \frac{12.69}{\mathrm{Re}_d^{2/3}(1 + B_M)}. \tag{23}$$

It can be shown that in the limit $k_l \to \infty$, Solution of Eq. (13) reduces to [137]:

$$T_d = T_g + (T_{d0} - T_g) \exp\left(-\frac{3ht}{c_l \rho_l R_d}\right), \tag{24}$$

where T_d is independent on R.

Eq. (24) was used in the previous kinetic models of DHE [4,10,11,51,52]. The present model is based on Eq. (13). The results predicted by the models based on both equations will be compared where appropriate.

The following approximations for dodecane are used [138]:

$$La = 37440 \cdot (T_{\text{cr}} - T_s)^{0.38} \quad \text{J/kg},$$

$$\rho_l = 744.11 - 0.771 \cdot (T - 300) \quad \text{kg/m}^3,$$

$$c_l = 2180 + 4.1 \cdot (T - 300) \quad \text{J/(kg} \cdot \text{K)},$$

where $T_{\text{cr}} = 659$ K is the critical temperature of n-dodecane. When calculating average liquid density and specific heat capacity, T in the last two expressions is replaced with the average temperature $\overline{T}$.

3.4.2. Knudsen layer

In kinetic region, which consists of two components, the evolution of molecular VDFs of air $f_a \equiv f_a(\mathbf{r}, t, \mathbf{v})$ and fuel vapour $f_v \equiv f_v(\mathbf{r}, t, \mathbf{v})$ is controlled by the corresponding Boltzmann equations [10,11,51,52]:

$$\left.\begin{aligned} \frac{\partial f_a}{\partial t} + \mathbf{v}_a \frac{\partial f_a}{\partial \mathbf{r}} &= J_{aa} + J_{av} \\ \frac{\partial f_v}{\partial t} + \mathbf{v}_v \frac{\partial f_v}{\partial \mathbf{r}} &= J_{va} + J_{vv} \end{aligned}\right\}, \tag{25}$$

where $J_{\alpha\beta}$ ($\alpha = a, v$; $\beta = a, v$) are collision integrals, taking into account the contribution of the collisions between molecules. The general numerical scheme used for the solution

Preprints (www.preprints.org) | NOT PEER-REVIEWED | Posted: 8 April 2022 doi:10.20944/preprints202204.0067.v1

of these equations, considering the effects of inelastic collisions, has been described in Sec. 3.3.

Eqs. (25) are solved subject to the boundary conditions at the interface between KL and the liquid phase and at the interface between KL and the vapour phase. The first boundary condition for fuel vapour can be presented as:

$$f_{v\,(\mathrm{out})} = \sigma f_{vs} + (1-\sigma) f_{vr}, \tag{26}$$

where f_{vs} is the distribution function of molecules leaving the liquid surface assuming that $\sigma = 1$, f_{vr} is the distribution function of reflected molecules. Both f_{vs} and f_{vr} are assumed to be isotropic Maxwellian. Eq. (26) is identical to Eq. (1). The temperature for f_{vs} is assumed to be equal to T_s, while the temperature for f_{vr} is assumed to be equal to T_{Rd}. This is justified by the fact that the thickness of the kinetic region is small and the gas temperature just above the droplet surface is close to T_{Rd} [139]. As introduced in Sec. 3.2, a more accurate approximation for f_{vr} would have been a bi-Maxwellian distribution, but this effect is not considered here.

At the boundary between the kinetic and hydrodynamic regions the distribution function of both fuel vapour and air molecules entering the kinetic region is assumed to be Maxwellian, controlled by ρ_{Rd} and T_{Rd}. Further details of the boundary conditions used for kinetic calculations were discussed by [11].

The contributions of both mass and heat transfer in KL are taken into account following the approach described in Ref. [51]. At first, as in Refs. [10,11,51,52], it is assumed that the evaporation coefficient σ_e is equal to 1. Then the effect of a realistic σ_e on DHE will be investigated.

3.4.3. Vapour region

In the fuel vapour region, it is assumed that the mass fluxes leaving KL and the corresponding diffusion fluxes in the vapour phase region are matched. This condition is presented in the form:

$$\frac{M_v}{N_A}\int_{-\infty}^{+\infty}\mathrm{d}v_y\int_{-\infty}^{+\infty}\mathrm{d}v_z\int_{0}^{+\infty}\mathrm{d}v_x v_x f_v(\mathbf{r},t,\mathbf{v}) = \frac{\rho_{\mathrm{mix}} D_{va}}{R_d}\ln(1+B_M) \equiv j_{\mathrm{h}} = j_v, \tag{27}$$

where ρ_{mix} is the density of the mixture of air and vapour at the inner boundary of the hydrodynamic region ($\rho_{\mathrm{mix}} = \rho_{vRd}/Y_{vRd}$), D_{va} is the binary diffusion coefficient (diffusion of vapour through air), and j_{h} is the mass flux of evaporated fuel. B_M considers the effect of the finite mass fraction of fuel vapour in the evaporation process. The binary diffusion coefficient is calculated from the following expression [140]:

$$D_{va} = 1.8583\times10^{-7}\sqrt{T_r^3\left(\frac{1}{M_v}+\frac{1}{M_a}\right)}\frac{1}{p\,\sigma_{va}^2\Omega_{D,va}}, \tag{28}$$

where D_{va} is in m^2/s, p is in atm, $\sigma_{va} = 0.5(\sigma_v+\sigma_a)$ is the average diameter of molecules of vapour and air, $\Omega_{D,va}$ is the function of $T^* \equiv k_B T_r/\varepsilon_{va}$, $\varepsilon_{va} = \sqrt{\varepsilon_v\varepsilon_a}$, ε_v and ε_a are Lennard-Jones parameters of fuel vapour and air [136], k_B is the Boltzmann constant, $T_r = T_s + \frac{1}{3}(T_g - T_s)$ is the reference temperature, T_s is the droplet surface temperature, and T_g is the ambient gas temperature.

Following [140], the following approximation for $\Omega_{D,va}$ is used:

$$\Omega_{D,va} = \frac{1.06036}{T^{*0.15610}} + \frac{0.19300}{\exp(0.47635T^*)} + \frac{1.03587}{\exp(1.52996T^*)} + \frac{1.76474}{\exp(3.89411T^*)}.$$

Following [51], the following values of parameters are used in most of our analysis: $\sigma_v = 9.373\times10^{-10}$ m, $\sigma_a = 3.667\times10^{-10}$ m, $\varepsilon_v/k_B = 351.0$ K, and $\varepsilon_a/k_B = 97.0$ K [136].

Preprints (www.preprints.org) | NOT PEER-REVIEWED | Posted: 8 April 2022 doi:10.20944/preprints202204.0067.v1

The heat flux supplied to the droplet is estimated as:

$$q_s = h(T_g - T_{Rd}), \tag{29}$$

where the convection heat transfer coefficient h is obtained from the equation:

$$h = \frac{k_{\text{mix}}}{R_d} \frac{\ln(1+B_T)}{B_T}, \tag{30}$$

k_{mix} is the thermal conductivity of the mixture of fuel vapour and air, B_T is the Spalding heat transfer number calculated as [3]:

$$B_T = (1+B_M)^{\varphi} - 1, \tag{31}$$

$$\varphi = \left(\frac{c_{pv}}{c_{pg}}\right) \frac{1}{\text{Le}} = \frac{c_{pv}\rho_{\text{mix}} D_{va}}{k_{\text{mix}}}, \tag{32}$$

688 Le $= k_{\text{mix}}/(c_{pg}\rho_{\text{mix}} D_{va})$ is the Lewis number, c_{pv} and c_{pg} are the specific heat capacities
689 of fuel vapour and ambient gas (air), respectively. Note that φ is independent on c_{pg}. Eq. (
690 32) is only valid for stationary droplets [136]. However, the average droplet temperatures
691 calculated using this formula are almost indistinguishable from the ones predicted by
692 the models considering the non-zero droplet velocities [141].

Following [51], the following approximations for c_{pv}, k_v and k_a are used

$$c_{pv} = 1594.60 + 1.15\tilde{T} - 100.56\tilde{T}^2 - 28.56\tilde{T}^3 + 5.07\tilde{T}^4 - 0.25\tilde{T}^5 \quad \text{J}/(\text{kg}\cdot\text{K}),$$

$$k_v = 0.02667 \cdot (T_r/300)) - 0.02087 \quad \text{W}/(\text{m}\cdot\text{K}),$$

$$k_a = 3.227 \times 10^{-3} + 8.3894 \times 10^{-5} T_r - 1.9858 \times 10^{-8} T_r^2 \quad \text{W}/(\text{m}\cdot\text{K}),$$

693 where $\tilde{T} = (T_r - 300)/300$.

The thermal conductivity of the mixture of fuel vapour and air is estimated as

$$k_{\text{mix}} = \sum_{i=1}^{2} \frac{X_i k_i}{\sum_{j=1}^{2} X_j \Phi_{ij}} \quad \text{W}/(\text{m}\cdot\text{K}),$$

where i and j stand for fuel vapour or air, and $X_{i,j}$ are molar fractions of the species,

$$\Phi_{ij} = \frac{1}{\sqrt{8}} \left(1 + \frac{M_i}{M_j}\right)^{-1/2} \left[1 + \left(\frac{k_i}{k_j}\right)^{1/2} \left(\frac{M_j}{M_i}\right)^{1/4}\right]^2,$$

694 $M_{i,j}$ are molar masses of the corresponding species ($M_v = 170.3$ kg/kmol, $M_a = 28.97$
695 kg/kmol) [136].

Following [51], the values of the saturated fuel vapour pressure are estimated as:

$$p_{v\,(\text{sat})} = A_1 \cdot \exp\left(\frac{T_s - A_0}{B_1}\right) \quad \text{Pa}, \tag{33}$$

where

$$\left.\begin{array}{l} A_0 = 300.17542 \\ A_1 = 70.44441 \\ B_1 = 22.36885 \end{array}\right\} \quad \text{when} \quad T_s < 440 \text{ K}$$

$$\left.\begin{array}{l} A_0 = 449.87125 \\ A_1 = 46204.48272 \\ B_1 = 56.97142 \end{array}\right\} \quad \text{when} \quad T_s \geq 440 \text{ K}.$$

696 Eq. (33) is an alternative presentation of the Clausius-Clapeyron equation [142].

Preprints (www.preprints.org) | NOT PEER-REVIEWED | Posted: 8 April 2022 doi:10.20944/preprints202204.0067.v1

The processes in kinetic and hydrodynamic regions are linked by the matching conditions of conservation of mass flux (see Eq. (27)) and heat fluxes at the interface

$$q_{\rm k} = q_{\rm h}, \tag{34}$$

Subscripts $_{\rm k}$ and $_{\rm h}$ refer to the kinetic and hydrodynamic regions, respectively.

Note that the above model for the hydrodynamic region will be reduced to a simplified version proposed in Ref. [51] if we assume that $\Omega_{D,va} = T^*$, $\varphi = 1$, $La = 250,000$ J/kg, $\rho_l = 586$ kg/m^3, $c_l = 2,900$ J/(kg K), and $k_{\rm mix} = 0.035$ J/(m K). These simplifications were justified by the fact that Ref. [51] focused on the comparison of the predictions of hydrodynamic and kinetic models rather than on the most accurate predictions of droplet radii and temperature during the heating and evaporation processes. In the present work, a considerably improved model is used as described above. The thermophysical properties of n-doedecane ($C_{12}H_{26}$) can be found in Ref. [138].

3.5. Droplet Heating and Evaporation (DHE) in Combustion Engines

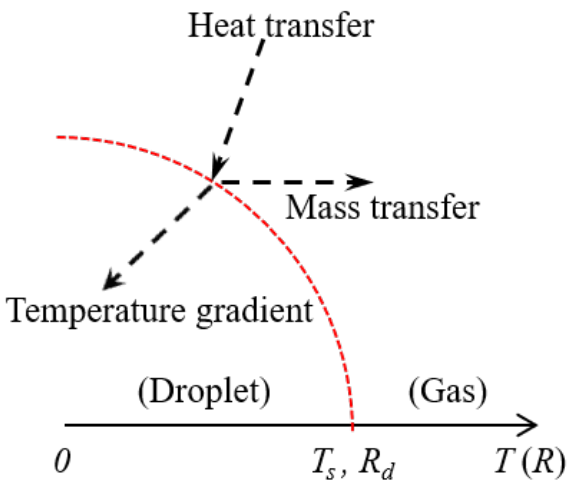

Figure 10. Heat and mass transfer processes in a droplet heating and evaporation (DHE) considering the temperature gradient inside.

The solution algorithm proposed in Ref. [51] is used to analyse the heat and mass transfer processes of DHE, as shown in Figure 10. The first step in the solution of Eqs. (25) is to perform an investigation of mass and heat transfer processes in KL for a set of values of ρ_{Rd} and T_{Rd}. Remembering that we consider the problem of DHE in a hot gas, these parameters are assumed to be in the ranges: $\rho_{Rd} < \rho_s$ and $T_{Rd} > T_s$. During the droplet heating process, the temperature decreases away from the droplet; the evaporation process is possible when the fuel vapour density decreases away from the droplet surface. Once the values of ρ_{Rd} and T_{Rd} are found, the solution of Eqs. (25) in KL enable us to calculate the normalised mass and heat fluxes at outer boundary of this region.

The algorithm was applied to estimate the surface temperature and lifetime of $C_{12}H_{26}$-DHE in hot gases of temperatures at 750 K, 1,000 K and 1,500 K. The initial droplet temperature and gas pressure in the three cases were assumed equal to 300 K and 30 bar, respectively. The initial droplet radius was 5 μm. The droplet was assumed to be stationary, but the effect of swelling was taken into account. The previously developed kinetic model for DHE into a high-pressure background gas (air) had been generalised to take into account the combined effects of inelastic collisions in the kinetic region, a realistic evaporation coefficient and temperature gradient inside droplets. Both ITC and ETC liquid phase models were used in the analysis. The effect of inelastic collisions was investigated based on the model introduced in Sec. 3.3. Both heat and mass transfer

Preprints (www.preprints.org) | NOT PEER-REVIEWED | Posted: 8 April 2022 doi:10.20944/preprints202204.0067.v1

in KL were considered. The boundary conditions at the outer boundary of the kinetic region were introduced by matching the mass fluxes of vapour leaving the kinetic region and entering into the surrounding hydrodynamic region, and the corresponding heat fluxes.

It was found that for the parameters typical for diesel engine-like conditions, the heat flux in the kinetic region is a linear function of the vapour temperature at the outer boundary of this region, but practically does not depend on vapour density at this boundary for all models [51], with or without the effect of inelastic collisions, and regardless of the effect of a non-unity evaporation coefficient. For any given temperature at the outer boundary of the kinetic region, the values of the heat flux was shown to decrease with the increasing number of internal degrees of freedom of the molecules. The rate of this decrease was shown to be strong for a small number of degrees of freedom but became negligible when the number of degrees of freedom exceeded 20. This enables us to restrict our analysis to only the first 20 arbitrarily chosen degrees of freedom of dodecane molecules without paying computational penalty when considering the effect of inelastic collisions.

The mass flux at this boundary was shown to decrease almost linearly with the increasing vapour density at the same location for all above-mentioned models. For any given vapour density at the outer boundary of the kinetic region, the mass flux was smaller for the model considering internal degrees of freedom than the one ignoring the inelastic collision. Remembering these properties of heat and mass fluxes and using the matching conditions at the outer boundary of kinetic region, the temperature and fuel vapour density at this boundary were found by following the procedure described in Ref. [51]. It was shown that the effect of inelastic collisions leads to a stronger increase in the predicted droplet evaporation time relative to the hydrodynamic model, compared with the similar increase predicted by the kinetic model considering only elastic collisions. The effect of a non-unity evaporation coefficient was shown to be weak at gas temperatures about or less than 1,000 K. These effects, however, had been shown to be noticeable for gas temperatures of 1,500 K. In all cases, the kinetic effect was shown to be negligible at the initial stage of DHE. At this stage, the surface temperature predicted by the ETC model was shown to be larger than that predicted by the ITC model, which was in agreement with the previous results [143].

4. Conclusions

4.1. Summary

Evaporation and condensation of fuel droplet (i.e., dodecane) can be investigated in MD simulations. The vapour-liquid coexisting curve is recovered and the thickness of the LV interface was predicted to be several manometers. The evaporation coefficient varied as a function of the liquid phase temperature, i.e., decreasing with the increasing of the liquid temperature. The estimated evaporation coefficient and VDF can be applied to analyse the exchange of the momentum and heat flux at the LV interface, which enables us to revisit the KBC at the interface of liquid and vapour such as KL.

The kinetic effect on DHE becomes pronounced when the drop radius is only several micrometres (i.e., 5μm). The non-equilibrium/rarefied gas dynamics cannot be assessed by the conventional fluid dynamics approach such as the Navier-Stokes-Fourier (NSF) equations. Instead, a particle method of solving the full Boltzmann equation can be an alternative. In addition, the contribution of the internal degree of freedom is noticeable in chain-like molecules such as dodecane. Therefore, a new approach to the solution of the Boltzmann equation is introduced to consider the inelastic collisions which redistribute the kinetic and internal energies of fuel molecules.

The numerical models mentioned above have been applied to the simulation of $C_{12}H_{26}$-DHE under IC engine conditions, including the effects of inelastic collisions in KL, a realistic evaporation coefficient at the LV interface and temperature gradient inside the droplet. It indicates that the effect of the inelastic collision in the kinetic

Preprints (www.preprints.org) | NOT PEER-REVIEWED | Posted: 8 April 2022 doi:10.20944/preprints202204.0067.v1

theory modelling leads to a stronger increase in the predicted droplet evaporation time compared to the conventional CFD solver. The effect of a realistic evaporation coefficient is also shown to be noticeable at a gas temperature of 1,500 K. In summary, it is recommended that a rigorous kinetic theory modelling of inelastic collisions alongside a realistic evaporation coefficient should be applied to accurately estimate the droplet surface temperature and its evaporation time under IC engine conditions.

4.2. Concluding Remarks

Droplet heating and evaporation (DHE) is a multi-physics, multi-scale and multi-phase phenomenon. This review establishes a new basis for the multi-scale modelling of fuel droplet heating and evaporation (MsM-$C_{12}H_{26}$-DHE) under IC engine conditions. The development of MsM-$C_{12}H_{26}$-DHE is threefold: MD estimates the evaporation coefficient and VDF of fuel molecules at the LV interface where a new KBC is built; Kinetic theory modelling of inelastic collisions alongside the KBC is used to describe the non-equilibrium gas dynamics of fuel vapour and gas mixture in KL; Heat and mass flux analysis of the fuel droplet under IC engine conditions is assessed after both effects of inelastic collisions in KL and a temperature-dependent evaporation coefficient at the LV interface are implemented.

This review has several impacts as follows:

i) It for the first considers the LV interface and inelastic effects of fuel vapour and gas mixture in combustion engine conditions (up to 30 bar and 1,500 K) within a consistent framework to unfold the underlying physics of heat and mass transfer phenomenon during DHE process.

ii) It has pushed the research of DHE from the hydrodynamics to the multiple scales, i.e., crossing macro, meso, and micro/nanoscales, which are relevant to cognate fields concerned with the fluid dynamics in bulk regions, non-equilibrium gas flows of fuel vapour and gas mixture in the vicinity of the droplet surface (i.e., KL), and the interfacial dynamics in-between them (i.e., LV).

iii) It provides an urgently needed simulation capability to quantify heating and evaporation of dodecane into nitrogen in IC engine conditions, in particular to predict the ultimate lifetime and surface temperature of fuel droplets for injection and ignition processes and make a direct and positive impact which will lead to far less pollution being emitted by heavy-duty vehicles (i.e., powertrains and lorries) and off-road carriers (i.e., ships).

Multi-scale modelling of DHE is not only applicable in internal combustion engines and gas turbines, but in many other industrial (evaporation cooling, surface coating, and lubrication solutions), medical (pharmaceutical drug manufacturing by spray drying, inhalers) and environmental applications (atmosphere flows, ocean sprays). For example, it will provide the in-depth knowledge and understanding of additive manufacturing (AM) and 3D printing technology. Moreover, the strategy of multi-scale modelling helps us stretch the challenges of fundamental fluid dynamics in inkjet printing (manipulating liquid jets and drops, jet break-up and drop formation dynamics in a drop-on-demand inkjet printing, spreading and breakup of nanodroplet impinging on a surface).

This work has developed a unique new capability in modelling $C_{12}H_{26}$-DHE at high-temperature and high-pressure conditions, which is relevant to the reduction of fuel consumption and CO_2 emissions in IC engines. It will enable us to make well-informed predictions of fuel droplet lifetime, and in turn help to assess the economic and environmental value of long-term low carbon emissions targeting carbon neutral; this is dedicated to investigating the environmental and socioeconomic impacts of low carbon vehicles compared to the electric or hybrid cars. This research will be a vital step towards developing multi-scale simulations for economical low carbon emission vehicles, especially when the major economies in the world to pass net zero emission laws to end its contribution to global warming by 2050.

Preprints (www.preprints.org) | NOT PEER-REVIEWED | Posted: 8 April 2022 doi:10.20944/preprints202204.0067.v1

Author Contributions: Writing—original draft preparation, J.X.; writing—review and editing, J.X.. All authors have read and agreed to the published version of the manuscript.

Funding: The APC was funded by the University of Derby.

Institutional Review Board Statement: Not applicable.

Informed Consent Statement: Not applicable.

Data Availability Statement: Data Availability Statements at https://www.mdpi.com/ethics.

Acknowledgments: J.X. thanks Professor Xin Bian from Zhejiang University for the useful discussions about the coupling library MUI.

Conflicts of Interest: The authors declare no conflict of interest.

Abbreviations

The following abbreviations are used in this manuscript:

MD	Molecular Dynamics
CGMD	Coarse Grain Molecular Dynamics
LV	Liquid-Vapour
DHE	Droplet Heating and Evaporation
CFD	Computational Fluid Dynamics
MC	Monte Carlo
KL	Knudsen Layer
MFP	Mean Free Path
VDF	Velocity Distribution Function
DDM	Domain Deposition Method
TST	Transition State Theory
ITC	Infinite Thermal Conductivity
ETC	Effective Thermal Conductivity
AM	Additive Manufacturing
FEM	Finite Element Method

References

1. Gold, M.; Higham, C.; Crua, C.; Shoba, T.; Heikal, M. High-Speed Microscopic Imaging of the Initial Stage of Diesel Spray Formation and Primary Breakup. SAE International, 2010.
2. Alexander, P.; Begg, S.M.; Heikal, M.R.; Li, G.; Gold, M. Airflow and fuel spray interaction in a gasoline DI engine. *SAE Technical Paper* **2005**, *01*, 2104.
3. Sazhin, S.S. Advanced models of fuel droplet heating and evaporation. *Energy Combust. Sci.* **2006**, *32*, 975–995.
4. Kryukov, A.P.; Levashov, V.Y.; Sazhin, S.S. Evaporation of diesel fuel droplets: kinetic versus hydrodynamic models. *Int. J. Heat Mass Transf.* **2004**, *47*, 2541–2549.
5. Crua, C. Combustion Processes in a Diesel Engine. PhD thesis, University of Brighton, School of Engineering, 2002.
6. Lefebvre, A.H. *Atomization and Sprays*; Hemisphere Publishing Corporation: New York, 1989.
7. Sazhin, S.S.; Shishkova, I.N.; Xie, J.F. Kinetic and molecular dynamics modelling of n-dodecane droplet heating and evaporation. Proceedings of ILASS Europe 2012, 12th Triennial Conference on Liquid Atomization and Spray Systems; , 2012.
8. Frezzotti, A. Boundary condition at the vapor-liquid interface. *Phys. Fluids* **2011**, *23*, 030609.
9. Tsuruta, T.; Nagayama, G. Molecular dynamics studies on the condensation coefficient of water. *J. Phys. Chem. B* **2004**, *108*, 1736–1743.
10. Shishkova, I.N.; Sazhin, S. A numerical algorithm of kinetic modelling of evaporation processes. *J. Comput. Phys.* **2006**, *218*, 635–653.
11. Sazhin, S.S.; Shishkova, I.N.; Kryukov, A.P.; Levashov, V.Y.; Heikal, M.R. Evaporation of droplets into a background gas: kinetic modelling. *Int. J. Heat Mass Transf.* **2007**, *50*, 2675–2691.
12. Cao, B.Y.; Xie, J.F.; Sazhin, S.S. Molecular dynamics study on evaporation and condensation of n-dodecane at liquid-vapour phase equilibria. *J. Chem. Phys.* **2011**, *134*, 164309.
13. Xie, J.F.; Sazhin, S.S.; Cao, B.Y. Molecular dynamics study of condensation/evaporation of Diesel fuel. Proceedings of ILASS Europe 2011, 24th European Conference on Liquid Atomization and Spray Systems; , 2011.
14. Bao, H.; Chen, J.; Gu, X.; Cao, B. A Review of Simulation Methods in Micro/Nanoscale Heat Conduction. *ES Energy & Environment* **2018**, *1*, 16–55.
15. Alfonsi, G. Reynolds-Averaged Navier,ÄìStokes Equations for Turbulence Modeling. *Applied Mechanics Reviews* **2009**, *62*.

Preprints (www.preprints.org) | NOT PEER-REVIEWED | Posted: 8 April 2022 doi:10.20944/preprints202204.0067.v1

16. Zhiyin, Y. Large-eddy simulation: Past, present and the future. *Chinese Journal of Aeronautics* **2015**, *28*, 11–24.
17. Wang, Y.; Yang, Y.; Yang, G.; Liu, C. DNS Study on Vortex and Vorticity in Late Boundary Layer Transition. *Communications in Computational Physics* **2017**, *22*, 441–459.
18. Li, C.; Xie, J. Numerical modeling of free surface flow over submerged and highly flexible vegetation. *Advances in Water Resources* **2011**, *34*, 468–477.
19. Shishkova, I.N.; Sazhin, S.S.; Xie, J.F. A solution of the Boltzmann equation in the presence of inelastic collisions. *J. Comput. Phys.* **2013**, *232*, 87–99.
20. Cheng-Wen, Z.; Jian-Fei, X.; Cong-Shan, Z.; Sheng-Wei, X.; Da-Chuan, Y. Simulation of natural convection under high magnetic field by means of the thermal lattice Boltzmann method. *Chinese Physics B* **2009**, *18*, 4083–4093.
21. Xie, J.F.; Cao, B.Y. Natural convection of power-law fluids under wall vibrations: A lattice Boltzmann study. *Numerical Heat Transfer, Part A: Applications* **2017**, *72*, 600–627.
22. Xie, J.F.; He, S.; Zu, Y.Q.; Lamy-Chappuis, B.; Yardley, B.W.D. Relative permeabilities of supercritical CO2 and brine in carbon sequestration by a two-phase lattice Boltzmann method. *Heat and Mass Transfer* **2017**, *53*, 2637–2649.
23. Xie, J.; Borg, M.K.; Gibelli, L.; Henrich, O.; Lockerby, D.A.; Reese, J.M. Effective mean free path and viscosity of confined gases. *Physics of Fluids* **2019**, *31*, 072002.
24. Xie, J.F.; Cao, B.Y. Nanochannel flow past permeable walls via molecular dynamics. *AIP Advances* **2016**, *6*, 075307.
25. Xie, J.F.; Cao, B.Y. Effect of various surface conditions on nanochannel flows past permeable walls. *Molecular Simulation* **2017**, *43*, 65–75.
26. Xie, J.F.; Cao, B.Y. Fast nanofluidics by travelling surface waves. *Microfluidics and Nanofluidics* **2017**, *21*, 111.
27. Xie, J.F.; Cao, B.Y. Influence of travelling surface waves on nanofluidic viscosity. *Computers & Fluids* **2018**, *160*, 42–50.
28. Rapaport, D.C. *The Art of Molecular Dynamics Simulation*; Cambridge University Press: Cambridge, 1995.
29. Martin, R.M. *Electronic Structure: Basic Theory and Practical Methods*; Cambridge University Press: Cambridge, 2004.
30. Esfarjani, K.; Chen, G.; Stokes, H.T. Heat transport in silicon from first-principles calculations. *Phys. Rev. B* **2011**, *84*, 085204.
31. Liu, T.H.; Zhou, J.; Liao, B.; Singh, D.J.; Chen, G. First-principles mode-by-mode analysis for electron-phonon scattering channels and mean free path spectra in GaAs. *Phys. Rev. B* **2017**, *95*, 075206.
32. Xu, Q.; Zhou, J.; Liu, T.H.; Chen, G. First-Principles Study of All Thermoelectric Properties of Si-Ge Alloys Showing Large Phonon Drag from 150 to 1100 K. *Phys. Rev. Applied* **2021**, *16*, 064052.
33. Cao, B.Y. Nonequilibrium molecular dynamics calculation of the thermal conductivity based on an improved relaxation scheme. *J. Chem. Phys.* **2008**, *129*, 074106.
34. Cao, B.Y.; Chen, M.; Guo, Z.Y. Temperature dependence of the tangential momentum accommodation coefficient for gases. *Appl. Phys. Lett.* **2005**, *86*, 091905.
35. Cao, B.Y.; Chen, M.; Guo, Z.Y. Liquid flow in surface-nanostructured channels studied by molecular dynamics simulation. *Phys. Rev. E* **2006**, *74*, 066311.
36. Cao, B.Y.; Guo, Z.Y. Equation of motion of phonon gas and non-Fourier heat conduction. *J. Appl. Phys.* **2007**, *102*, 053503.
37. Carravetta, V.; Clementi, E. Water water interaction potential: An approximation of the electron correlation contribution by a functional of the SCF density matrix. *J. Chem. Phys.* **1984**, *81*, 2646–2651.
38. Berendsen, H.J.C.; Grigera, J.R.; Straatsma, T.P. The missing term in effective pair potentials. *J. Phys. Chem.* **1987**, *91*, 6269–6271.
39. Jorgensen, W.L.; Madura, J.D.; Swenson, C.J. Optimized intermolecular potential functions for liquid hydrocarbons. *J. Am. Chem. Soc.* **1984**, *106*, 6638–6646.
40. de Pablo, J.J.; Laso, M.; Siepmann, J.I.; Suter, U.W. Continuum-configurational-bias Monte Carlo simulations of long-chain alkanes. *Mol. Phys.* **1993**, *80*, 55–63.
41. Toxvaerd, S. Molecular dynamics calculation of the equation of state of alkanes. *J. Chem. Phys.* **1990**, *93*, 4290–4295.
42. Padilla, P.; Toxvaerd, S. Self-diffusion in n-alkane fluid models. *J. Chem. Phys.* **1991**, *94*, 5650–5654.
43. Smit, B.; Karaborni, S.; Siepmann, J.I. Computer simulations of vapour-liquid phase equilibria of n-alkanes. *J. Chem. Phys.* **1995**, *102*, 2126–2140.
44. Simon, J.M.; Kjelstrup, S.; Bedeaux, D.; Hafskjold, B. Thermal flux through a surface of n-octane. A non-equilibrium molecular dynamics study. *J. Phys. Chem.* **2004**, *108*, 7186–7195.
45. Simon, J.M.; Bedeaux, D.; Kjelstrup, S.; Xu, J.; Johannessen, E. Interface film resistivities for heat and mass transfers-integral relations verified by non-equilibrium molecular dynamics. *J. Phys. Chem.* **2006**, *110*, 18528–18536.
46. Harris, J.G. Liquid vapour interface of alkane oligomers-structure and thermodynamics from molecular-dynamics simulations of chemically realistic models. *J. Phys. Chem.* **1992**, *96*, 5077–5086.
47. Ibergay, C.; Ghoufi, A.; Goujon, F.; Ungerer, P.; Boutin, A.; Rousseau, B.; Malfreyt, P. Molecular simulations of the n-alkane liquid-vapour interface interfacial properties and their long range corrections. *Phys. Rev. E* **2007**, *75*, 051602.
48. Zahn, D. Length-dependent nucleation mechanism rule the vapourization of n-alkane. *Chem. Phys. Lett.* **2008**, *467*, 80–83.
49. Amat, M.A.; Rutledge, G.C. Liquid-vapor equilibria and interfacial properties of n-alkanes and perfluoroalkanes by molecular simulation. *J. Chem. Phys.* **2010**, *132*, 114704.
50. Mizuguchi, H.; Nagayama, G.; Tsuruta, T. Molecular dynamics study on evaporation coefficient of biodiesel fuel. Seventh International Conference on Flow Dynamics; , 2010.

Preprints (www.preprints.org) | NOT PEER-REVIEWED | Posted: 8 April 2022 doi:10.20944/preprints202204.0067.v1

51. Sazhin, S.S.; Shishkova, I.N. A kinetic algorithm for modelling the droplet evaporation process in the presence of heat flux and background gas. *Atomization Sprays* **2009**, *19*, 473–489.
52. Sazhin, S.S.; Shishkova, I.N.; Heikal, M. Kinetic modelling of fuel droplet heating and evaporation: calculations and approximations. *Int. J of Eng. Sys. Model. Simul.* **2010**, *2*, 169–176.
53. Tsige, M.; Patnaik, S. An all-atom simulation study of the ordering of liquid squalane near a solid surface. *Chem. Phys. Lett.* **2008**, *457*, 357–361.
54. Tsuruta, T.; Tanaka, H.; Masuoka, T. Condensation/evaporation coefficient and velocity distributions at liquid-vapour interface. *Int. J. Mass Heat Transf.* **1999**, *42*, 4107–4116.
55. Anisimov, S.I.; Dunikov, D.O.; Zhakhovskii, V.V.; Malyshenko, S.P. Properties of a liquid-vapor interface at high-rate evaporation. *J. Chem. Phys.* **1999**, *110*, 8722–8729.
56. Nagayama, G.; Tsuruta, T. A general expression for the condensation coefficient based on transition state theory and molecular dynamics simulation. *J. Chem. Phys.* **2003**, *118*, 1392–1399.
57. Nagayama, G.; Matsuo, M.; Tsuruta, T. Nonequilibrium Molecular Dynamics Study on Interface Heat and Mass Transfer. Proceedings of the 13th International Heat Transfer Conference; , 2006.
58. Cercignani, C. *The Boltzmann Equation and Its Application*; Springer-Verlag: Berlin, 1988.
59. Meland, R. Molecular exchange and its influence on the condensation coefficient. *J. Chem. Phys.* **2002**, *117*, 7254–7258.
60. Meland, R.; Ytehus, T. Boundary condition at a gas-liquid interphase. 22nd Internaltional Sysposium of Rarefied Gas Dynamics; , 2001.
61. Ishiyama, T.; Yano, T.; Fujikawa, S. Kinetic boundary condition at a vapour-liquid interface. *Phys. Rev. Lett.* **2005**, *95*, 084504.
62. Ishiyama, T.; Yano, T.; Fujikawa, S. Molecular dynamics study of kinetic boundary conditions at an interface between argon vapor and its condensed phase. *Phys. Fluids* **2004**, *16*, 2899–2906.
63. Ishiyama, T.; Yano, T.; Fujikawa, S. Molecular dynamics study of kinetic boundary conditions at an interface between a polyatomic vapor and its condensed phase. *Phys. Fluids* **2004**, *16*, 4713–4726.
64. Landau, L.D.; Lifshitz, E. *Statistical Physics*; Pergamon Press: Oxford, 1980.
65. Akhiezer, A.I.; Akhiezer, I.A.; Polovin, P.V.; Sitenko, A.G.; Stepanov, K.N. *Plasma Electrodynamics*; Nauka Publishing House: Moscow, 1974.
66. Grad, H. On the kinetic theory of rarefied gases. *Comm. Pure Appl. Math.* **1949**, *2*, 331–407.
67. Bhatnagar, P.L.; Gross, E.; Krook, M. A model for collision processes in gases 1. Small amplitude processes in charged and neutralone component systems. *Phys. Rev.* **1954**, *94*, 511–525.
68. Sazhin, S.S. Cyclotron whistler-mode instability in a collisional plasma. *Geomagnetic Research* **1978**, *23*, 105–107.
69. Igoshin, V.I.; Kurochkin, V.I. Laser vaporisation of a metal in a gaseous atmosphere. *Sov. J. Quant. Electron* **1984**, *14*, 1049.
70. Shakhov, E.M. *Methods of Investigation of Rarefied Gas Dynamics*; Nauka Publishing House: Moscow, 1974.
71. Lifshitz, E.M.; Pitaevski, L.P. *Physical Kinetics*; Nauka Publishing House: Moscow, 1979.
72. Rose, J. Interphase matter transfer, the condensation coefficient and dropwise condensation. Proceedings of 11st International Heat Transfer Conference; , 1998.
73. Tcheremissine, F.G. Direct numerical solution of the Boltzmann equation. Proceedings of the 25th International Symposium on Rarefied Gas Dynamics; , 2006.
74. Yen, S.M. Numerical Solution of the Nonlinear Boltzmann Equation for Nonequilibrium Gas Flow Problems. *Ann. Rev. Fluid Mech.* **1984**, *16*, 67–97.
75. Bird, G.A. *Molecular Gas Dynamics and the Direct Simulation of Gas Flows*; Oxford University Press: Oxford, 1994.
76. Aristov, V.V.; Tcheremissine, F.G. *Direct numerical solution of the Boltzmann equation*; Computer Centre of Russia Academy of Sciences: Moscow, 1992.
77. Aristov, V.V.; Kryukov, A.P.; Tcheremissine, F.G.; Shishkova, I. Solution of the Boltzmann equation for a plane jet with condensation on a cryogenic panel. *J. Comput. Math. Math. Phys.* **1991**, *30*, 1093–1099.
78. Aristov, V.V.; Tcheremissine, F.G.; Shishkova, I.N. Solution of the Boltzmann equations for study of inclined shock wave reflection. 18th International Symposium on Rarefied Gas Dynamics; , 1992.
79. Tcheremissine, F.G. Conservative evaluation of Boltzmann collision integral in discrete ordinates approximation. *Comput. Math. Appl.* **1998**, *35*, 215–221.
80. Tcheremissine, F.G. Discrete approximation and examples of the solution of the Boltzmann equation. Computational Dynamics of Rarefied Gases; , 2000.
81. Aristov, V.V.; Popov, S.P.; Tcheremissine, F.G.; Shishkova, I. Numerical solution of the Boltzmann and Navier-Stokes equations for a plannar jet impinging on a cooled surface. *Comput. Math. Math. Phys.* **1997**, *37*, 239–242.
82. Aoki, K.; Takata, S.; Kosuge, S. Vapor flows caused by evaporation and condensation on two parallel plane surfaces: effect of the presence of a noncondensable gas. *Phys. Fluids* **1998**, *10*, 1519–1533.
83. Kosuge, S.; Aoki, K.; Takata, S. Shock-wave structure for a binary gas mixture: finite-difference analysis of the Boltzmann equation for hard-sphere molecules. *Eur. J. Mech. B* **2001**, *20*, 87–126.
84. Taguchi, S.; Aoki, K.; Takata, S. Vapor flows condensing at incidence onto a plane condensed phase in the presence of noncondensable gas. I. Subsonic condensation. *Phys. Fluids* **2003**, *15*, 689–705.

Preprints (www.preprints.org) | NOT PEER-REVIEWED | Posted: 8 April 2022 doi:10.20944/preprints202204.0067.v1

85. Taguchi, S.; Aoki, K.; Takata, S. Vapor flows condensing at incidence onto a plane condensed phase in the presence of noncondensable gas. II. Supersonic condensation. *Phys. Fluids* **2004**, *16*, 79–92.
86. Raines, A. Study of a shock wave structure in a gas mixture on the basis of the Boltzmann equation. *Eur. J. Mech. B* **2002**, *21*, 599–610.
87. Kryukov, A.P.; Levashov, V.Y.; Shishkova, I.N. Condensation in the presence of a non-condensable component. *J. Eng. Phys. Thermophys.* **2005**, *78*, 15.
88. Kryukov, A.P.; Yastrebov, A.K. Analysis of transport processes in a vapour film during the interaction between a heated body with cold liquid. *Therm. Phys. High Temp.* **2003**, *41*, 771.
89. Borgnakke, C.; Larsen, P.S. Statistical collision model for Monte Carlo simulation of polyatomic gas mixture. *J. Comput. Phys.* **1975**, *18*, 405–420.
90. Kondo, T.; Okada, R.; Mori, D.; Yamamoto, S. Inelastic scattering process of H_2O on Pt(111) studied by supersonic molecular beam techniques. 22nd European Conference on Surface Science (ECOSS 22); , 2004.
91. Tilinin, I.S. Impact-parameter dependence of inelastic energy losses in slow atom-atom collisions. *Nuclear instruments and Methods in Phys. Research B* **1996**, *115*, 102–105.
92. Ferrari, L.; Carbognani, A. Differential kinetic equations for a Rayleigh gas with inelastic collisions. *Physica A* **1998**, *251*, 452–468.
93. Benedetto, D.; Caglioti, E. The collapse phenomenon in one-dimensional inelastic point particle systems. *Physica D* **1999**, *132*, 457–475.
94. Biben, T.; Martin, P.A.; Piasecki, J. Stationary state of thermostated inelastic hard spheres. *Physica A* **2002**, *310*, 308–324.
95. Banasiak, J.; Groppi, M. Solvability of linear kinetic equations with multi-energetic inelastic scattering. *Reports on Math. Phys.* **2003**, *52*, 235–253.
96. Fournier, N.; Mischler, S. A spatially homogeneous Boltzmann equation for elastic, inelastic and coalescing collisions. *J. Math. Pure. Appl.* **2005**, *84*, 1173–1234.
97. Santos, A. A simple model kinetic equation for inelastic Maxwell particles. Proceedings of the 25th International Symposium on Rarefied Gas Dynamics; , 2006.
98. Sizhuk, A.; Yezhov, S. The dynamic theory for the inelastically colliding particles. *J. Mole. Liquids* **2006**, *127*, 84–86.
99. Lambiotte, R.; Ausloos, M.; Brenig, L.; Salazar, J.M. Energy and number of collision fluctuations in inelastic gases. *Physica A* **2007**, *375*, 227–232.
100. Kremer, G.M.; Silva, A.W.; Alves, G.M. On inelastic reactive collisions in kinetic theory of chemically reacting gas mixtures. *Physica A* **2010**, *389*, 2708–2718.
101. Furioli, G.; Pulvirenti, A.; Terraneo, E.; Toscani, G. Convergence to self-similarity for the Boltzmann equation for strongly inelastic Maxwell molecules. *Ann. I. H. Poincar´e AN* **2010**, *27*, 719–737.
102. Wang-Chang, C.W.; Uhlenbeck, G.E. *Transport Phenomena in Polyatomic Gases*; University of Michigan: Ann Arbor, 1951.
103. Mores, T.F. Kinetic Model for Gases with Internal Degrees of Freedom. *Phys. Fluids* **1964**, *7*, 159–169.
104. Cheremisin, F.G. Solution of the Wang-Chang-Uhlenbeck Master Equation. *Doklady Physics* **2002**, *47*, 872–875.
105. Frezzotti, A.; Ytrehus, T. Kinetic theory study of steady condesation of a polyatomic gas. *Phys. Fluids* **2006**, *18*, 027101.
106. Holway, L.H. New statistical models for kinetic theory. *Phys. Fluids* **1966**, *9*, 1658–1673.
107. Frezzotti, A. A numerical investigation of the steady evapotaion of a polyatomic gas. *Eur. J. Mech. B/Fluids* **2007**, *26*, 93–104.
108. Bian, X.; Praprotnik, M., Domain Decomposition Methods for Multiscale Modeling. In *Handbook of Materials Modeling: Applications: Current and Emerging Materials*; Andreoni, W.; Yip, S., Eds.; Springer International Publishing: Cham, 2018; pp. 1–21.
109. Tang, Y.H.; Kudo, S.; Bian, X.; Li, Z.; Karniadakis, G.E. Multiscale Universal Interface: A concurrent framework for coupling heterogeneous solvers. *Journal of Computational Physics* **2015**, *297*, 13–31.
110. Allen, M.P.; Tildesley, D.J. *Computer Simulation of Liquids*; Clarendon: Oxford, 1987.
111. van der Ploeg, P.; Berendsen, H.J.C. Molecular dynamics simulation of a bilayer membrane. *J. Chem. Phys.* **1982**, *76*, 3271–3276.
112. Xie, J.F.; Sazhin, S.S.; Cao, B.Y. Molecular dynamics study of the processes in the invinicy of the n-dodecane vapour/liquid interphase. *Phys. Fluids* **2011**, *23*, 112104.
113. Ryckaert, J.P.; Ciccotti, G.; Berendsen, H.J.C. Numerical integration of the cartesian equations of motion of a system with constraints: molecular dynamics of n-alkanes. *J. Comput. Phys.* **1977**, *23*, 327–341.
114. Maxwell, J.B. *Data Book on Hydrocarbons: Application to Process Engineering*; Van Nostrand: Princeton, 1955.
115. Kawamata, M.; Yamamoto, T. Molecular dynamics simulation of surface ordering in liquid n-alkanes. *J. Phys. Soc. Jpn.* **1997**, *66*, 2350–2354.
116. Pierce, F.; Tsige, M.; Borodin, O.; Perahia, D.; Grest, G.S. Interfacial properties of semifluorinated alkane diblock copolymers. *J. Chem. Phys.* **2008**, *128*, 214903.
117. Marek, R.; Straub, J. Analysis of the evaporation coefficient and the condensation coefficient of water. *Int. J. Heat Mass Transf.* **2001**, *44*, 39–53.
118. Gladstone, G.; Laidler, K.; Eyring, H. *The Theory of Rate Processes*; McGraw-Hill: New York, 1941.
119. Sazhin, S.S.; Wild, P.; Leys, C.; Teobaert, D.; Sazhina, E.M. The three temperature model for the fast-axial-flow CO_2 laser. *Physics D: Applied Physcis* **1993**, *26*, 1872–1883.
120. Xie, J.F.; Sazhin, S.S.; Cao, B.Y. Molecular dynamics study of condensation/evaporation and velocity distribution of n-dodecane at liquid-vapour phase equilibria. *J. Therm. Sci. Tech.* **2012**, *7*, 288–300.

Preprints (www.preprints.org) | NOT PEER-REVIEWED | Posted: 8 April 2022 doi:10.20944/preprints202204.0067.v1

121. Xie, J.F.; Sazhin, S.S.; Cao, B.Y. Molecular dynamics study of condensation/evaporation and velocity distribution of Diesel fuel at liquid-vapour phase equilibria. the 3rd Asian Symposium on Computational Heat Transfer and Fluid Flow; , 2011.
122. Santos, A. Transport coefficients of d-dimensional inelastic Maxwell models. *Physica A* **2003**, *321*, 442–466.
123. Koura, K. Improved null-collision technique in the direct simulation Monte Carlo method: Application to vibrational relaxation of Nitrogen. *Computers Math. Appl.* **1998**, *35*, 139–154.
124. Flynn, P.F.; Durrett, R.P.; Hunter, G.L.; zur Loye, A.O.; Akinyemi, O.C.; Dec, J.E.; Westbrook, C.K. Diesel combustion: an integrated view combining laser diagnostics, chemical kinetics, and empirical validation. *SAE report* **1999**, *01*, 0509.
125. Stiesch, G. *Modelling Engine Sprays and Combustion Processes*; Springer: London, 2003.
126. Bertoli, C.; Migliaccio, M.N. A finite conductivity model for diesel spray evaporation computations. *Int. J. Heat Mass Transf.* **1999**, *20*, 552–561.
127. Maqua, C.; Castanet, G.; Grisch, F.; Lemoine, F.; Kristyadi, T.; Sazhin, S.S. Monodisperse droplet heating and evaporation: experimental study and modelling. *Int. J. Heat Mass Transf.* **2008**, *51*, 3932–3945.
128. Kristyadi, T.; Deprédurand, V.; Castanet, G.; Lemoine, L.; Sazhin, S.S.; Elwardany, A.; Sazhina, E.M.; Heikal, M.R. Monodisperse monocomponent fuel droplet heating and evaporation. *Fuel* **2010**, *89*, 3995–4001.
129. Sazhin, S.S.; Krutitskii, P.A.; Gusev, I.G.; Heikal, M.R. Transient heating of an evaporating droplet. *Int. J. Heat Mass Transf.* **2010**, *53*, 2886–2836.
130. Mitchell, S.L.; Vynnycky, M.; Gusev, I.G.; Sazhin, S.S. An accurate numerical solution for the transient heating of an evaporating spherical droplet. *Applied Mathematics and Computation* **2011**, *217*, 9219–9233.
131. Sazhin, S.S.; Krutitskii, P.A.; Gusev, I.G.; Heikal, M.R. Transient heating of an evaporating droplet with presumed time evolution of its radius. *Int. J. Heat Mass Transf.* **2011**, *54*, 1278–1288.
132. Sazhin, S.S.; Krutitskii, P.A.; Gusev, I.G.; Heikal, M.R. Transient heating of a semitransparent spherical body immersed into a gas with inhomogeneous temperature distribution. *Int. J. Therm. Sci.* **2011**, *50*, 1278–1288.
133. Kartashov, E.M. *Analytical Methods in the Thermal Conductivity Theory of Solids*; Vyshaya Shkola: Moscow, 2001.
134. Carslaw, H.S.; Jaeger, J.C. *Conduction of Heat in Solids*; Clarendon Press: Oxford, 1986.
135. Sazhin, S.S.; Krutitskii, P.A.; Abdelghaffar, W.A.; Mikhalovsky, S.V.; Meikle, S.T.; Heikal, M.R. Transient heating of diesel fuel droplets. *Int. J. Heat Mass Transf.* **2004**, *47*, 3327–3340.
136. Abramzon, B.; Sirignano, W. Droplet vaporization model for spray combustion calculations. *Int. J. Heat Mass Transf.* **1989**, *32*, 1605–1618.
137. Sazhin, S.S.; Krutitskii, P.A. A conduction model for transient heating of fuel droplets. Proceedings of the 3rd International ISAAC; , 2003.
138. Abramzon, B.; Sazhin, S. Convective vaporization of fuel droplets with thermal radiation absorption. *Fuel* **2006**, *85*, 32–46.
139. Fuchs, N.A. *Evaporation and Droplet Growth in Gaseous Media*; Pergamon Press: Lodon, 1959.
140. Bird, R.B.; Stewart, W.E.; Lightfoot, E.N. *Transport Phenomena*; John Wiley & Sons: England, 2002.
141. Elwardany, A.E.; Gusev, I.G.; Castanet, G.; Lemoine, F.; Sazhin, S.S. Mono- and multi-component droplet cooling/heating and evaporation: comparative analysis of numerical models. *Atomization Sprays* **2011**, *21*, 907–931.
142. Atkins, P.; de Paula, J. *Atkins' Physical Chemistry*; Oxford University Press: Oxford, 2002.
143. Sazhin, S.S.; Kristyadi, T.; Abdelghaffar, W.A.; Heikal, M.R. Models for fuel droplet heating and evaporation: comparative analysis. *Fuel* **2006**, *85*, 1613–1630.